

UC San Diego

UC San Diego Electronic Theses and Dissertations

Title

A mantle source for epithermal gold mineralization in the Northern Nevada Rift

Permalink

<https://escholarship.org/uc/item/9w2633x1>

Author

Maria-Benavides, Jennifer

Publication Date

2018

Supplemental Material

<https://escholarship.org/uc/item/9w2633x1#supplemental>

Peer reviewed|Thesis/dissertation

UNIVERSITY OF CALIFORNIA SAN DIEGO

A mantle source for epithermal gold mineralization in the
Northern Nevada Rift

A thesis submitted in partial satisfaction of the
requirements for the degree
Master of Science

in

Earth Sciences

by

Jennifer Maria-Benavides

Committee in charge:

James M.D. Day, Chair
Steven Constable
Geoffrey W. Cook

2018

Copyright

Jennifer Maria-Benavides, 2018

All rights reserved.

The thesis of Jennifer Maria-Benavides is approved, and it is acceptable
in quality and form for publication on microfilm and electronically:

Chair

University of California San Diego

2018

TABLE OF CONTENTS

Signature Page	iii
Table of Contents	iv
List of Figures	vi
List of Tables	vii
Acknowledgements	viii
Abstract of the Thesis	ix
Introduction	1
1.1. Geological Setting	6
1.2. Local geology	10
1.3. Previous work	12
2. Methods & Samples	13
2.1. Samples	13
2.2. Mineral Chemistry	14
2.3. Whole rock major- and trace- element analyses	14
2.4. Rhenium-osmium isotope and HSE abundance analyses	15
2.5. Analytical standard development for gold measurements	17
3. Results	21
3.1. Results for Fire Creek country rocks	21
3.1.1. Whole rock major- and trace- element concentrations	21
3.1.2. Highly siderophile element abundances	26
3.1.3. ^{187}Re - ^{187}Os isotope systematics of host rocks	26
3.2. Results for electrum grains	29
3.2.1. Electrum composition by LA-ICP-MS	29
3.2.2. Highly siderophile element abundances	31
3.2.3. ^{187}Re - ^{187}Os isotope systematics of electrum grains	31
4. Discussion	33
4.1. Geochemistry and alteration of host rocks	33
4.2. Differences and similarities between LA-ICP-MS analyses and isotope dilution	35

4.3. Crustal contamination and relation to the Columbia River flood basalts	37
4.4. Source of electrum and implications for ore genesis	39
4.5. Age of electrum	43
5. Conclusions	43
Appendix	44
References	44

LIST OF FIGURES

Figure 1: Map of the northwestern United States	5
Figure 2: Columbia River Flood Basalt volume and age distribution	9
Figure 3: General stratigraphy of the Fire Creek mine	11
Figure 4: Laser Ablation ICP-MS patterns for a JM-reef sulfide grain	18
Figure 5: Total-alkali versus silica diagram for Fire Creek volcanic rocks	19
Figure 6: Harker diagrams of major element abundance variations	20
Figure 7: Incompatible trace element and rare earth element plots for country rocks	23
Figure 8: Incompatible trace element and rare earth element plots for the dike	24
Figure 9: La/Sm versus La/Yb plot	25
Figure 10: Highly siderophile element diagram for host rocks	27
Figure 11: ^{187}Re - ^{187}Os isotope diagram for host rocks	28
Figure 12: Laser Ablation ICP-MS patterns for electrum	30
Figure 13: Highly siderophile element diagram for electrum measured by ID TIMS and ICP-MS	32
Figure 14: Highly siderophile element diagram for electrum measured by ID TIMS and ICP-MS compared to LA-ICP-MS data	35
Figure 15: ^{187}Re - ^{187}Os isotope diagram for electrum grains	36
Figure 16: ^{187}Re - ^{187}Os isotope diagram for host rocks compared with Columbia River flood basalts	38
Figure 17: ^{187}Re - ^{187}Os isotope models for (a) heterogeneity and (b) disturbance	42

LIST OF TABLES

Table 1: Geochronology of bonanza Au-Ag Deposits, Northern Great Basin (modified from Saunders et al., 2008).	4
Table 2: Laser-ablation ICP-MS data (ppm) for standard reference materials, Hoba, Filomena and Coahuila	51
Table 3: Major and trace element compositions of Fire Creek whole-rock samples determined by X-ray fluorescence and ICP-MS	52
Table 4: Osmium isotope and HSE abundances (pg) for total analytical blanks	54
Table 5: Analysis of in-house metal and sulfide standards versus recommended values	55
Table 6: Laser-ablation ICP-MS data (in ppm) for sulfide samples from JM Reef at the Stillwater Mine, MT	56
Table 7: Full ^{187}Re - ^{187}Os isotope and highly siderophile element abundances (ppb) for Fire Creek electrum and country rocks	57
Table 8: Laser-ablation ICP-MS data (in ppm) for gold samples from the Fire Creek Mine, NV	58

ACKNOWLEDGEMENTS

I dedicate this thesis with my deepest gratitude and affection to my family, who helped me in all things great and small. Moving 2,105 km away from home is the toughest change I have had to endure. I am greatly indebted to my sixth grade teacher, Mrs. Martha Rodriguez, who helped me adapt to a new culture, taught me a new language, and firmly told me she expected great things from me. I have since lost contact, but without her kindness, encouragement, and inspiration I would not have embraced my potential. I would like to recognize Dr. Jacqueline Azize-Brewer, the California Louis Stokes Alliance for Minority Participation (CAMP) in Science, Engineering, and Mathematics, and the Upward Bound Programs, whom instilled strong work ethic and provided guidance through all of my education.

It is without question that this project and educational experience would be possible without the guidance of an incredible mentor, Dr. James Day. I offer my gratitude and appreciation to him for helping me grow both as a person and researcher, the unforgettable field excursions, and trusting support. Thank you to my committee members, Dr. Geoff Cook, I admire your kindness and devotion to education, and Dr. Steven Constable. To all my Professors, I could never think about my experience at Scripps Institution of Oceanography without a sense of accomplishment and fulfillment thanks to you.

The members of the Scripps Isotope Geochemistry Laboratory are rare gems. I would not have loved working in the lab without Emily Pringle as a teacher. Thanks to Marine Paquet for helping me with my column chemistry and TIMS analysis. Ruan Hattingh, thanks for staying long work days with me during my sample analysis (and for bringing Georgie). Warm thanks to Carrie McIntosh and Brian Oller who have provided unconditional support since I joined this lab, I could not have done it without them. Thanks to Eric Snortum for bringing joy and happiness everywhere he goes. To Christy Liang, thanks for listening to my bad jokes over the years and offering endless help. Nicole Phelan thanks for loving Ophie and your transcending friendship. This journey has had long stressful nights, busy week days and weekends, but it has also had joyful moments, heart-fastening discoveries, and rewards. Loving thanks to Carlos Anguiano because he has been a supportive of me through every step of the way. You always believed I could do anything, even when I had doubts, and you continue to encourage me every day.

ABSTRACT OF THE THESIS

A mantle source for epithermal gold mineralization in the Northern Nevada Rift

by

Jennifer Maria-Benavides

Master of Science in Earth Sciences

University of California San Diego, 2018

Professor James M.D. Day, Chair

Gold is a noble metal that has fueled mineral resource exploration in the Northern Great Basin and profoundly affected the national economy. The origin of the gold deposits has been at the center of basic and applied research, with the goal to develop refined exploration models. For the first time, I am able to unambiguously constrain the nature of electrum from a low-sulfidation epithermal deposit in the Northern Nevada Rift. In this study, the highly siderophile elements (HSE; Os, Ir, Ru, Rh, Pt, Pd, Re and Au) serve as an innovative tracing tool due to the inherent relationship between the HSE and Au that can be used to trace the origin of electrum directly. Coupled precise $^{187}\text{Os}/^{188}\text{Os}$ compositions and isotope dilution HSE abundance data are reported for electrum grains from the Fire Creek Mine, as well as for a suite of host rocks that encompass the bimodal basalt-rhyolite volcanism of northern Nevada. The mid-Miocene bimodal host-rocks have Os isotope compositions consistent with crustal contamination observed in the Columbia

River Flood Basalt (CRFB) province. The host rocks are isotopically similar to the CRFB Wannapum, Grande Ronde, and Imnaha basalt formations. Highly siderophile element concentrations are heavily fractionated for the host rocks but are less fractionated for the electrum. Rhenium-Osmium isotope analysis of electrum yields a relatively unradiogenic initial $^{187}\text{Os}/^{188}\text{Os}$ of 0.1588, demonstrating a source distinct from the crust and that can only be of mantle origin. From this, I estimate that as much as 96% of the gold in the Fire Creek deposit is of mantle origin, in contrast to evidence for much larger crustal contributions from proxy measurements.

1. Introduction

Gold has been a valued commodity for over 8000 years, largely by virtue of its stability as a virtually inert noble metal (Harvey & Day, 2016). The discovery of gold during the ‘California Gold Rush’ of the 1850’s set the United States on its trajectory as the world’s leading economy. In 1900, the U.S. committed to a gold standard economy for the second time since 1792, with the gold dollar becoming the standard unit of account (Elwell, 2011). Consequently, the value of the US dollar was tied to the supply of gold, establishing a trust enabling global trade, and the establishment of a Federal Reserve (Friedman, 1963). When World War I broke out, the exorbitant costs forced most of the world to suspend the gold standard. “Balance-of-payment” deficits contributed to the end of a pure gold standard in 1933 (Eichengreen, 1992). With the value of gold rising, individuals began to exchange their US dollars for gold, consequently depleting the U.S. gold reserves. In 1934, the Gold Reserves Act was enacted, prohibiting private ownership of gold except with an approved license (Elwell, 2011). In return the new American currency was on a quasi-gold standard (devalued ~60% from the pure gold standard) leading to inflation (Elwell, 2011). In the 1970’s, the gold standard was abandoned by President Nixon opening the next phase of gold in the free market.

Gold has been central to the world economy, not because of its economic value or aesthetics, but because of its supply. Scientific investigation of gold is partly driven by the need to interpret the nature of diverse deposit types and their complex geology, in order to establish new viable deposits. The causes for the distribution gold and the genesis of economically viable deposits, however, remains poorly understood.

Gold is found naturally either as native gold or more commonly as “electrum,” an Au-Ag alloy with traces of other metals (e.g., Pt, Pd, Os, Ir, Ru, Rh, Cu, Hg; Gammons and Williams-Jones, 1995). There are two primary reasons why gold mineralization is not well-understood. First, Au differs from other transition metals, and its coordination chemistry is still under-developed. Briefly, double coordination compounds of Au(I) are well characterized, as opposed to coordination compounds Au(III) and Au(I and III), with Au(II) and Au(V) fostering little to no interest in the field of chemistry (Nekrasov, 1996). Experimental investigations have shown that the most favorable conditions for crystallization of high-grade gold requires sulfide solutions

with H₂S ligands and low pH (Nekrasov, 1996). Thus, further understanding of Au cluster compound processes would be pivotal to understanding the source of gold mineralization and chemical processes.

The second reason is that the source(s) of the gold are not well constrained. Initial efforts to understand gold mineralization were facilitated by advancements in applications of stable O- and H- isotopes during the 1950's. Stable isotope investigations began to document in detail the interactions of hydrothermal and geothermal fluids leading to the isotopic exchange of such fluids and the host rocks of bonanza ore vein deposits (Craig et al., 1956; Rye, 1966; Taylor, 1973). Bonanza ore vein are sought after due to the exceptionally high-grade ore content. From interpretations using these techniques, a model that still prevails today was developed. Magmas are viewed as the heat source that drove convection of heated meteoric water, which leached metals and other chemical constituents from local rocks and deposited them; this model is otherwise called the "leaching model" (Nash et al., 1995). During the 1990's the magmatic contribution to the formation of hydrothermal ore deposits was proposed and investigations were launched to understand a variety of deposits in the Northern Great Basin (Hedenquist and Lowenstern, 1994; Saunders and Schoenly, 1995). In particular, investigations using laser-ablation inductively coupled plasma mass spectrometry (LA-ICP-MS) of brine and vapor fluid inclusions in quartz derived from low density magmatic fluids, by Günther et al. (1998) and Heinrich (1999), confirmed that magmatic fluids contributed significantly to shallow vein deposits.

Stable isotope investigations, for the most part, interpret that the majority of gold and silver was leached from the underlying sedimentary units (John et al., 2003; Tosdal et al., 2003). Here, the magma source served as a heat source that drove low sulfidation epithermal system hydrothermal activity and leached the metals from the sedimentary deposits. Although stable isotopes constrain an origin and role of the fluids in the formation of epithermal deposits, they do not identify the source of the gold.

Pettke and Frei, (1996) identified that gold is usually alloyed with Ag and/or Cu and therefore must also contain trace levels of Pb. Based on this information, Pb isotope ratios served

as a semi-direct way to measure ore minerals. Lead isotope investigations for numerous Northern Nevada Rift (NNR) deposits have been performed and found that the gold, vein silicate minerals, and the local volcanic and sedimentary rocks did not provide conclusive evidence for the relation to one another or to the source of the gold (Kamenov et al., 2007). Gangue minerals appear to derive from local Mesozoic metasedimentary rocks from the region, but the gold itself was similar to Miocene volcanic rocks from the region. As a result, they proposed that the epithermal ores were exsolved from magmatic fluids by the magmas themselves and Pb isotopes were ultimately used to link mid-Miocene bimodal basalt-rhyolite hosted ores to the emergence of the Yellowstone Hotspot track (Kamenov et al., 2007).

Studies of the geology, age, and attributes of low-sulfidation gold-silver deposits in northern Nevada document both similarities and differences (Pirajno, 2009; Vikre, 1985; Noble et al., 1988; Sillitoe et al., 1996; John, 2001; John et al., 2003; Wallace, 2003; Kamenov et al., 2007; Saunders et al., 2008; Hammes et al., 2009). A method using laser $^{40}\text{Ar}/^{39}\text{Ar}$ incremental heating of adularia has been used to refine age estimates of low sulfidation epithermal deposits in the Northern Great Basin and have generally found that the majority of NNR epithermal gold deposits formed between 16.5 and 15.5 Ma, contemporaneous to basaltic volcanism of the Steens Mountains (Figure 2; Hammes et al., 2009). From this information, a model has been established in which magma chambers of basalt fed bimodal volcanism in the Northern Nevada rift, with the majority of low sulfidation epithermal deposits coming from rhyolite magma chambers. The heat from these chambers generated shallow geothermal systems to form and concentrate Au-Ag ores that evolved from episodically released hydrothermally-driven fluids (Hammes et al., 2009; Perez, 2013).

Despite numerous studies focusing extensive resources to examine gold mineralization, none have been able to unambiguously identify a source for the gold (Kamenov et al., 2007; Saunders et al., 2010). The Fire Creek Deposit is host to epithermal electrum mineralization with as much as 69.5 wt.% Au and 26.6 wt.% Ag (Perez, 2013). Here, I present petrology, major-, trace- and highly siderophile elements for the Fire Creek Deposit, offering a detailed chemical analysis of electrum and the rocks that host them. With these data, I establish a direct chemical relation of the low sulfidation Au-Ag epithermal deposit at the Fire Creek with a

mantle source. This was achieved in two distinct steps. First, I improved understanding of the standardization of laser ablation analysis for gold and metal alloys by quantifying precision measurements of reference metal standards via solution ICP-MS. An attempt to develop a sulfide standard for gold proved difficult due to heterogeneity of the proposed standard, but this has also prompted further work. The second phase of the study involved the analysis of country rocks for comparison with direct measurement of the electrum for highly siderophile element abundances and $^{187}\text{Re}/^{188}\text{Os}$. It is this latter step that has enabled me to unambiguously determine the source of gold for the first time.

Table 1 : Geochronology of bonanza Au-Ag Deposits, Northern Great Basin (modified from Saunders et al., 2008).

Deposit	Age (Ma)	Host Rock	References
Sleeper	16.1-14.3 ± 0.07	Rhyolite	Conrad et al., 1993
Midas	15.4-15.3± 0.08	Rhyolite	Leavitt et al., 2004
Fire Creek	16.11-15.86±0.08	Basalt	Millard et al., 2018 (<i>unpublished</i>)
Mule Canyon	15.6 ± 0.04	Basalt	John et al., 2003
Buckhorn	15.0 ± 0.04	Basalt	Wells et al., 1971
Hog Ranch	15.2-14.8± 0.04	Rhyolite	Bussey, 1996
Ivanhoe	15.19± 0.05	Rhyolite	Wallace, 2003
Buckskin National	15.8-15.5± 0.2	Rhyolite	Vikre, 1985
Buckskin-National	16.06± 0.3	Rhyolite	Vikre, 2007
DeLamar(ID)	15.7± 0.5	Rhyolite	Halsor et al., 1988
War Eagle Mtn. I (ID)	16.31± 0.04	Granitoid	Hames et al., 2009
War Eagle Mtn. II (ID)	15.61± 0.04	Granitoid	Hames et al., 2009
Jumbo	16.53± 0.04	Metasediments	Kamenov et al., 2007
Sandman	16.17± 0.04	Metasediments	Kamenov et al., 2007
Tenmile	16.03± 0.03	Metasediments	Kamenov et al., 2007
New Alma	16.03±0.03	Meta-sediments	Kamenov et al., 2007
McDermitt (Hg deposit)	15.6±0.4	Rhyolite	Noble et al., 1988
Seven Troughs	13.82± 0.02	Rhyolite	Hudson et al., 2006

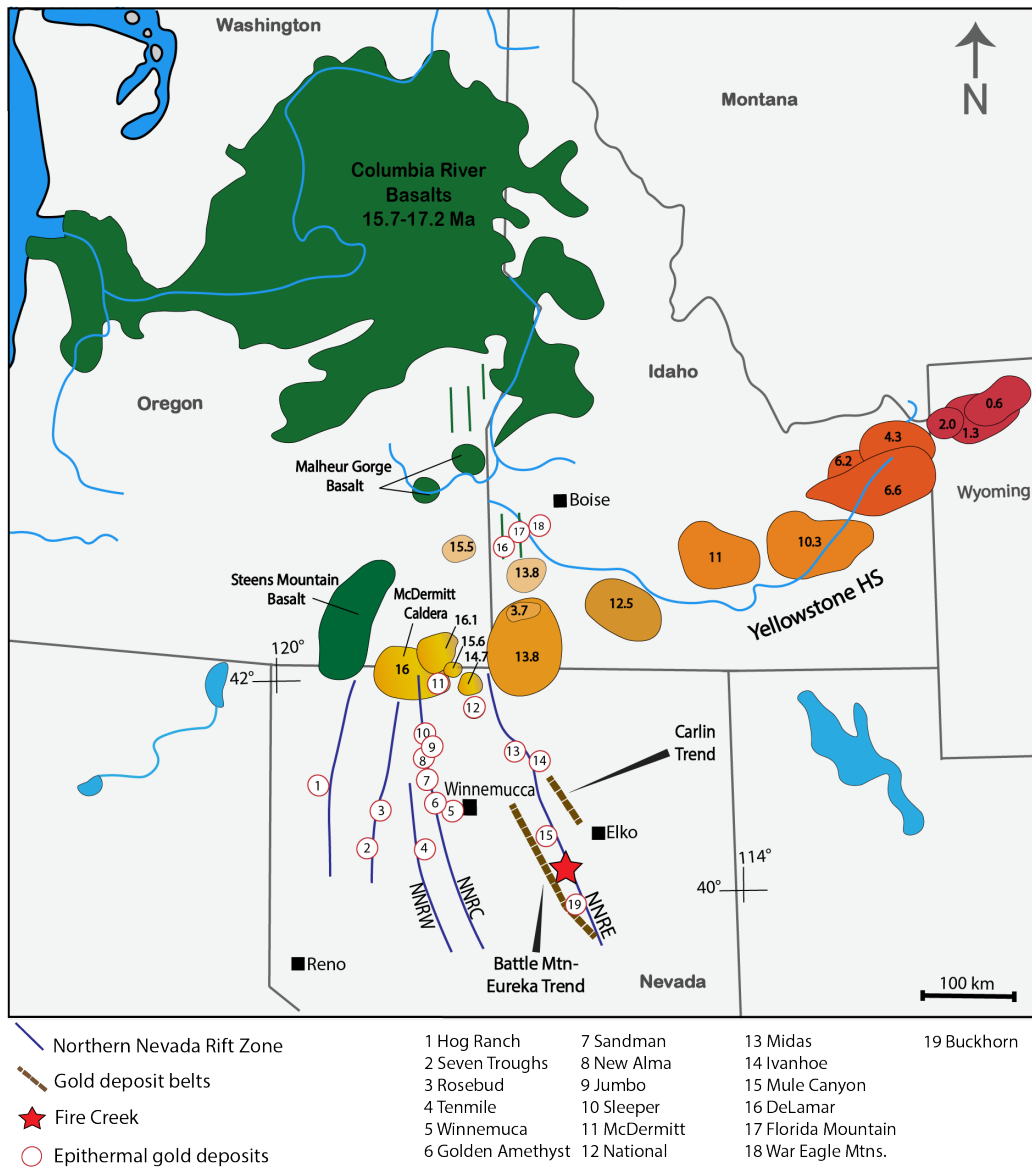


Figure 1: Map of Northwestern United States, highlighting the distribution of mid-Miocene volcanism unrelated to arc volcanism, including Columbia River Basalts (CRB), Yellowstone Hotspot track with their respective ages, the Northern Nevada Rift (NRR) and locations for 17-14 Ma low sulfidation epithermal deposits (modified from Saunders et al., 2008). The Fire Creek Mine lies along the NNR- East, in proximity to the Mule Canyon Deposit and between the Carlin Trend and Battle Mtn.- Eureka Trend. See also Table 1.

Geological Background

1.1. Geologic Setting

The Northern Great Basin (NGB) contains a large number of mineral deposits host to important mineral resources such as barite, silver, copper, beryllium, lithium, rare-earth elements, zinc and gold. It is composed of a diverse assemblage of gold deposits and complex geologic environments including Carlin-type, porphyry, distal disseminated, sedimentary-exhalative, and epithermal deposits (John et al., 2003a; Hofstra and Wallace, 2006). Porphyry Cu-(Mo)-Au deposits are magmatic hydrothermal systems that typically relate to subduction and are generated by the injection of oxidized magmas saturated with metal-rich fluids (Sun et al., 2015). Distal disseminated deposits are sedimentary rock hosted Au-Ag deposits that form by precipitation of metals from hydrothermal fluids distal to intrusive bodies with their own magmatic-hydrothermal systems, usually porphyry, skarn or polymetallic veins (Model 19c of Cox and Singer, 1990, 1992; Theodore, 1998). Sedimentary-exhalative deposits are hosted in marine sedimentary rocks and form from vented ore-bearing hydrothermal fluids that mix with a water reservoir to precipitate minerals with stratiform character (Large et al., 1981). Carlin-type are gold deposits that resemble the style of mineralization from the Carlin trend, which are large hydrothermal replacement Au-Ag deposits hosted primarily by Paleozoic miogeoclinal carbonate rocks, or as disseminated deposits (Cline et al., 2005; Muntean et al., 2011).

Cenozoic magmatism in the Northern Great Basin began during the Eocene to early Miocene with the emplacement of ‘interior’ andesite-rhyolite deposits. The eruption of dacite to rhyolite ash-flow tuffs, flow dome complexes, and andesitic to dacitic lava flows formed the Tuscarora magmatic belt, extending southeastward from northeastern California to the interior of the continental margin arc in central Utah (John, 2001; Christensen and Yeats, 1992; Best et al., 1999). Deposit types include Cu-Mo porphyry, skarn, and several epithermal deposits. Notably, the interior andesite-rhyolite overlaps in space with both the western andesite and the bimodal basalt-rhyolite assemblage (John, 2001). Carlin-type gold deposits are associated temporally with the mid-Tertiary, subduction related magmas and crustal extension (John et al., 2003A). Despite being explained as subduction related magmas, a strong argument for partial mixing of mantle

derived basalts and crust has been proposed based on the temporal and spatial association with crustal extension (Morris et al., 2001; Feely and Gnder, 1991; John, 2001).

The dynamic magmatic environment in the North American west during the mid-Cenozoic is evident by distinct volcanic assemblages and respective ore emplacement. The western andesite assemblage is a calc-alkaline series found in parts of eastern California and western Nevada, that formed in a continental-arc environment from subduction of oceanic crust from 22 Ma to 4 Ma (Christiansen and Lipman, 1972). This subduction-related magmatism led to the first ore emplacement of Cu, Mo, Au deposits, and W skarns, with porphyry Cu-Au and high sulfidation Au-Ag being unique to the assemblage (John, 2001). Intense subduction-related calc-alkaline magmatism through the Middle and Late Jurassic, the Cretaceous, and the Mid-Cenozoic was significant leading to the formation of these deposits (Christiansen and Yeats, 1992; John, 2001). The bimodal basalt-rhyolite assemblage represents an abrupt change in the style of volcanism in the Northern Great Basin; this is a tholeiitic to mildly alkaline basalt series related to Basin and Range extension.

Intraplate bimodal basalt-rhyolite magmatism initiated during continental rifting around 17 Ma in the NNR, contemporary to the impingement of the Yellowstone Hotspot on the west North American Plate, and continues today (Atwater, 1970; Dickinson and Snyder, 1978; Camp and Ross, 2004; John and Wallace, 2000). Thermal weakening of the crust led to moderate extension in northern Nevada through the Tertiary until wide spreading of the Basin and Range occurred between 16.5 to 15 Ma (John et al., 2003; John and Wallace, 2000; Theodore et al., 1998; Zoback and Thompson, 1978). This large-scale extension was contemporaneous to early volcanism in the NNR, dike intrusions, initial rhyolite volcanism at the southwestern end of the Yellowstone-Snake River Plain hotspot track, and the eruption of the Steens Basalt (Figure 2; Camp et al., 2015). The rift is broken into three separate arrays where low-sulfidation Au-Ag epithermal deposits formed and are commonly found in felsic volcanic rocks, in the form of bonanza veins (Figure 1). Gold mineralization ages from numerous Au-Ag deposits in NNR fall between 16.5 to 15 Ma, with recent $^{40}\text{Ar}/^{39}\text{Ar}$ dating of adularia bands, from the multiple mineralization veins at the Fire Creek deposit, showing ore emplacement here occurred between ~16.0-15.9 Ma (Millard et al., 2018). The Fire Creek, Mule Canyon, and Buckhorn basalt-hosted

deposits (Table 1) lie between Carlin-type deposits, while the Ivanhoe Hg District and Buckhorn Au-Ag district intersect the Carlin and Battle Mountain-Eureka trends which were emplaced ~ 42 to 36 Ma (Figure 1; Cline et al., 2007; Wallace, 2003; John and Wallace 2000).

The NNR is the surface manifestation of crustal extension during the Miocene with a north-northwest-trending aeromagnetic anomalies which extends 500 km southeast from the Nevada-Oregon state boundary to the southeast Nevada-Arizona state boundary (John and Wallace, 2000; Zoback and Thompson, 1978). Various authors have interpreted these anomalies as pre-Cenozoic, deep crustal faults that served as conduits for southward propagation of basaltic dike swarms associated with flood basalt volcanism (Zoback and Thompson, 1984; Robinson, 1970; John, 2001; Ponce and Glen, 2008). Consequently, these basaltic dikes must have supplied magma for bimodal volcanic centers that host epithermal Au-Ag deposits in the NNR concurrent with the impingement of the Yellowstone Hotspot (Zoback and Thompson, 1978; Zoback et al., 1994). Low-sulfidation epithermal deposits are all located within the Northern Nevada Rift, which is thought to have led to localization of these ores (Figure 1; John, 2001; Ponce and Glen, 2002; Leavitt et al., 2004). Based on temporal, spatial, and structural relationships of bimodal volcanism and low sulfidation Au-Ag epithermal mineralization, these deposits formed concurrently with the CRBF and possess an intrinsic relationship to the emergence of the Yellowstone Hotspot. Recent investigations suggest that Yellowstone Hotspot magmas that formed the CRBF and the dikes that supplied epithermal ore are linked, yet there remains debate about their mechanism and origin. Disagreement persists since no singular model can account for all aspects of mid-Miocene magmatism and extension. Several models involving plume and non-plume interactions have been investigated (Camp et al., 2013), and all involve a component of magma ascending and penetrating the continental crust as a result of a slab breaking mechanism (Geist & Richards, 1993; Liu & Stegman, 2012; Camp et al., 2015; Perez, 2013).

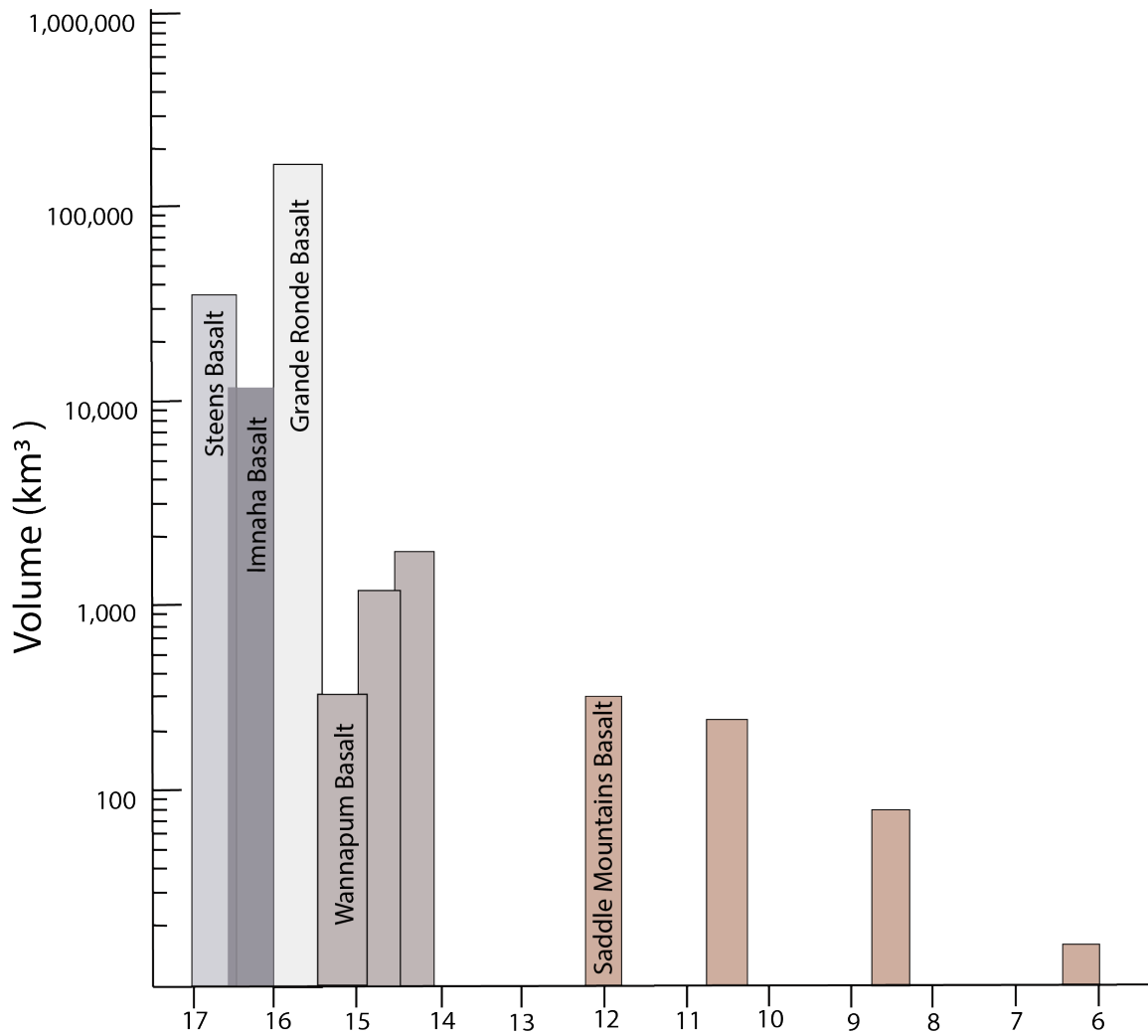


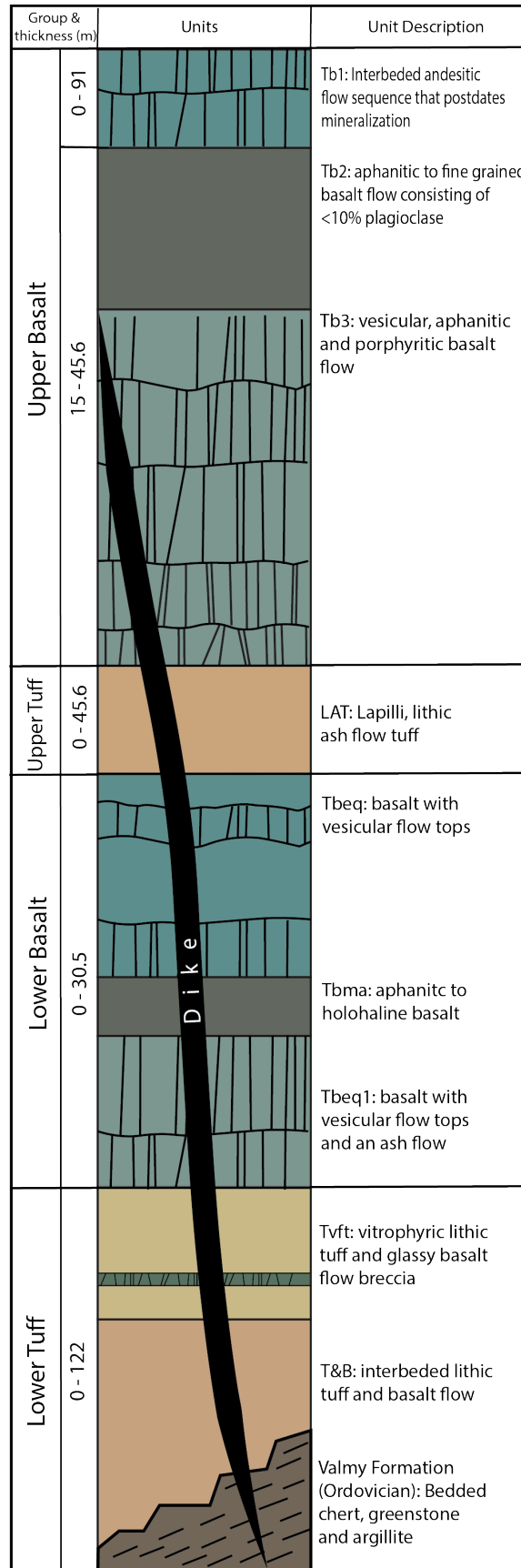
Figure 2: Volume (km³) against Age (Ma) diagram for the Columbia River Basalt Formations. Included are ages from ~17 to ~6 Ma and flow volume for Steens Basalt (Swisher et al., 1990; Reidel et al., 2013), Imnaha Basalt (Camp et al., 2003), Grande Ronde Basalt (Hooper et al., 2002; Reidel et al., 2013), Wannapum Basalt (Tolan et al., 1989), and Saddle Mountains Basalt (Tolan et

1.2. Local Geology

The Fire Creek Deposit is currently an active underground mine operated by Klondex Mines Limited and is located north of the Shoshone Range. In the northern Shoshone Range, basement rocks consist of Ordovician, Silurian and Devonian deep-water marine, siliciclastic sedimentary rocks (John et al., 2003). Unconformably overlying the basement are the early Oligocene Cetano Tuff and mid-Tertiary sequence of sedimentary rocks consisting of coarse debris flows, conglomerates, siltstone, mudstone and minor fresh-water limestone that were deposited prior to the onset of mid-Miocene rifting (John et al. 2003a, 2000). The Fire Creek Mine is composed of a series of basaltic to andesitic mid-Miocene lava flows intruded by dikes of basalt to andesitic composition. Gold-silver mineralization is found either as shallow fault-controlled gold in altered Tertiary basaltic host rocks, or as native gold occurring in quartz-calcite veins or structures in basalt host dikes (Odell et al., 2018). All surface and below-ground mapped geologic units at the Fire Creek are host to significant low sulfidation epithermal Au-Ag vein type ore deposits.

General stratigraphy at the Fire Creek has been reported by Odell et al. (2018). Fire Creek geology consists mainly of two distinct series; one of Miocene basalts, andesite, dacite flows, and the other of tuffs and pyroclastic flows that overlie clastic sediments (Figure 3). From here on, they will be referred by their series group. The upper basalt unit consists of basalt flows (Tb1, Tb2, Tb3), the upper tuff unit is a lapilli lithic-ash tuff (LAT), the lower basalt unit consists of equigranular basalts (Tbeq, Tbeq1, Tbma), and the lower tuff unit consists of tuffaceous sediments and volcanics (Tvft, T&B), and the Valmy Formation which has ceded chert, greenstone and argillite (Odell et al., 2018). Trachydacite cap rock (Tb1) unconformably overlies mafic rocks and serves as the only surface unit that post-dates Au-Ag mineralization (Perez, 2013).

Figure 3: General stratigraphy for the Fire Creek Mine. Units are grouped into upper basalt, upper tuff, lower basalt, and lower tuff. Unit thickness for the units are listed in meters (m) and generalized unit descriptions are included. Unit descriptions and relative order are as described by Raven et al. (2011) and Perez (2013).



1.3. Previous work

The Fire Creek Property has gone through a series of exploration stages by Klondex Mines Ltd., which acquired ownership in the 1980s. A series of technical reports that recall a general property description, geology, history and mineral exploration estimate have been released since 2006. The specific set of samples used in this study were recovered from the 2011 surface exploration program and were used in a previous study implementing a whole-rock to mineral scale analysis of epithermal gold mineralization at the Fire Creek Deposit (Perez, 2013). Findings reported focused on highly siderophile element (HSE) analysis using *in-situ* laser-ablation inductively coupled plasma mass spectrometry analysis coupled with textural observations, and are relevant to this study, being referenced throughout the text. I also reference recent Klondex technical reports (Odell et al., 2013; Odell et al., 2015; Odell et al., 2018).

Work by Perez (2013) reported a detailed whole rock to mineral scale investigation to establish ore paragenesis at the basalt hosted Au-Ag epithermal deposit. The investigation presented the first known highly siderophile element analysis on electrum grains with *in situ* chemical analysis and coupled textural observations. Whole rock major element compositions and field observations allowed identification of multiple dike events of andesitic and mafic magmas emplaced, resembling an enriched mantle composition. Petrographic observations coupled with highly siderophile element abundances of the electrum grains identified that the Fire Creek Deposit experienced episodic fluid ore emplacement events which produced Au and Ag in the form of Au-Ag bearing sulfide phases, and as high-grade ore electrum. Laser ablation ICP-MS of one electrum (FC 50-1) and sulfide grain reported by Perez (2013), from the same polished thin-section, identified strong evidence to suggest that observed alloy and sulfide fractionation became increasingly enriched in Au from ligand transport but may ultimately have been derived from a mantle source.

2. Methods and Samples

2.1. Samples

Twenty-four whole-rock samples representative of the local geology at the Fire Creek and four distinct veins of electrum mineralized in quartz-calcite veins were analyzed in this study. Fire Creek mineralization has previously been characterized using semi-quantitative analysis performed with Scanning Electron Microscopy (SEM), quantitative mineral chemistry using Electron Probe Micro-Analysis (EPMA), and whole rock geochemistry using X-ray fluorescence (XRF), following the procedures outlined in Boyd & Mertzman (1987) (see Perez, 2013). Here, I applied laser ablation ICP-MS of electrum grains, solution-based ICP-MS determination of trace-element abundance in whole rocks, and determination of Os isotope compositions and highly siderophile element abundances (Os, Ir, Ru, Pt, Pd, Re) by negative-ion thermal ionization mass spectrometry (N-TIMS) and isotope dilution ICP-MS methodologies for both electrum grains and whole rocks. All work presented in this thesis was done at the Scripps Isotope Geochemistry Laboratory (SIGL).

Cores and surface samples in this study were collected from the Fire Creek Property, Lander County, Nevada in 2011. Two core holes, and representative intervals within the cores, FC 0703 (depth of 274-281 m) and FC 0427 (depth of 548.64 m), encompass the lithological diversity, degree of alteration, and mineralization observed at the Fire Creek Property. FC 0703 represents the main mineralization zone, which contains both high-grade and low-grade Au-Ag ore. Gold sampling was recovered within a 1.2 m high-grade ore-section of FC 0703, and are labeled according to the Klondex labeling system. FC 0427 sampled non-mineralized to slightly mineralized sections. Samples collected at surface exposures are representative of sub-surface and surface lithology (1102-A, 1102-B, 1104, 1106, 1108, 1109, 1110), and correspond to bimodal volcanism in the area.

2.2. Mineral Chemistry

Concentration measurements for the highly siderophile elements were determined on electrum grains in three polished sections (FC 50-2-2, FC 50-1-3-1, FC 50 1-3-2) and one rock sample (FC 50-2-1) using *in-situ* laser ablation inductive coupled mass spectrometry (LA-ICP-MS) at the SIGL. Electrum grain compositions were determined using a *New Wave Research UP213* (213 nm) laser-ablation system coupled to a *ThermoScientific* iCap Qc Inductively Coupled Plasma-Mass Spectrometer by monitoring ^{101}Ru , ^{103}Rh , ^{106}Pd , ^{85}Re , ^{191}Ir , ^{192}Os , ^{196}Pt and ^{197}Au , as well as other elements (e.g., ^{57}Fe , ^{63}Cu). Electrum phases were analyzed using ablation spots with a 50 and 100 μm beam diameter, a laser repetition rate of 5 Hz, and a photon fluence of 3.5 to 4 J/cm^2 . The sample was introduced to a 3 cm^3 ablation cell, in a sample holding stage, where laser ablation took place. Each analysis consisted of 60 seconds of data collection, with 20 second background sample gas data collection, leading to 40 seconds of laser ablation of the sample. Washout time between analysis was 120 seconds. To enhance production and transport of fine aerosols the cell was flushed with a He-gas flow and was mixed with an Ar carrier gas flow at ~ 1 L/min before reaching the torch. Data were collected in time-resolved mode to observe compositional variation in the sample surface so that effects of inclusions, mineral zoning, and possible penetration of laser beam to underlying phases could be evaluated. For each analysis, plots of counts per second versus time were examined and integration intervals for the gas background and the sample analysis were selected manually. Standardization was performed using our in-house preferred values for iron meteorite reference materials, Hoba, Filomena, Coahuila and our newly developed JM-Reef sulfide standard. Analyses gave precisions better than 30% (RSD) for all elements listed excluding Au, which was close to detection saturation. All standard values for laser-ablation analysis are compiled in Table 2.

2.3. Whole rock major- and trace- element analyses

Major element abundances were analyzed at Franklin & Marshall College where samples were analyzed for major element oxides, selected trace element abundances, loss on ignition (LOI), and $\text{Fe}^{2+/3+}$ using a PW2403 Panalytical, Inc. XRF vacuum spectrometer, following procedures outlined in Boyd & Mertzman (1987). Major element peak and background

measurements yield an uncertainty of <0.1 wt% and for trace elements standards yield an uncertainty of < 5%. These data were previously reported in Perez (2013).

To measure whole-rock trace elemental abundances, I used solution based ICP-MS. Whole rocks were ground into fine powders using an agate mortar and pestle. Trace element abundances were determined by digesting 100 mg of sample powder prior to analysis by ICP-MS using a *ThermoScientific iCAP Qc quadruple* ICP-MS in standard mode using methods outlined in Day et al. (2014). Samples, standard reference materials and blanks were initially digested at 150°C in optima grade concentrated 4 mL HF to 1 mL HNO₃ for >72 hrs on a hotplate. Resulting solutions were dried down and reacted twice with TD HNO₃ to break down fluorides, followed by dilution of clear sample solutions by a factor of 5000 in 2% HNO₃ and doping with a 1 ppb indium solution to monitor instrumental drift. International reference materials (BHVO-2 #1955, BIR-1, BIR-2, DTS-2B #0506) were analyzed as unknowns along with samples, to assess matrix matching, external reproducibility, and accuracy. Sample blanks were monitored to ensure data quality. Reproducibility of the reference materials for trace elements was better than 5%, with the exception of Th, U, Pb, Ta, Zn, Cu, Ni, Mn, Cr, V, Ti, Li (6-8%) and W (10%) (Table 3).

2.4. Rhenium-Osmium isotope and HSE abundance analyses

Highly siderophile element abundance analysis in Fire Creek whole rocks were performed at the SIGL using 1 g of well-homogenized powdered samples that were sealed in long borosilicate Carius tubes in preparation for a standard acid digestion Carius tube method (Day et al., 2016). In addition to the sample powder, Carius tubes were loaded with the appropriate amounts of isotopically enriched multi-element spike (¹⁸⁵Re, ¹⁰⁶Pd, ¹⁹⁴Pt, ¹⁹¹Ir, ⁹⁹Ru, ¹⁹⁰Os), and an acid mixture of 1:1.75 Aqua Regia (11 mL total). For electrum analyses, smaller masses of material (~20-50 mg) were measured and spiking was done by using the laser ablation ICP-MS data for electrum samples. The electrum grains were hand separated and then treated in 6M HCl for 5 minutes until only visible electrum was present (no adhering calcite, quartz, or sulfide).

Samples were digested in Carius tubes at a temperature of 270°C in a convection oven for >72 hrs. After digestion, the liquid and undigested silicate material were transferred into 50 mL

centrifuge tubes. Osmium was triply extracted from the acid phase into CCl₄ and then back-extracted from the solvent into concentrated HBr (Cohen and Waters, 1996). Two micro-distillations were performed to recover highly purified Os (Birck et al., 1997). Purified osmium was used for negative ion mode *ThermoScientific* Triton thermal ionization mass spectrometry where isotopic compositions of Os were measured as OsO₃⁻ ions. Raw Os data was corrected off-line for an oxide interference, mass fractionation using $^{192}\text{Os}/^{188}\text{Os} = 3.08271$, ^{190}Os spike additions and Os procedural blank contributions. The UMCP Johnson-Matthey standard (35 pg Os) was used to track $^{187}\text{Os}/^{188}\text{Os}$ precision during the analytical procedure with precision of better than $\pm 0.2\%$ (2SD; 0.11369 ± 0.00022 ; n=6).

Rhenium and the other HSE were recovered and purified from the residual Aqua Regia solutions using standard anion exchange column separation techniques (Day et al. 2016). The separation procedure involves loading 1 cm³ of pre-cleaned Bio-Rad AGI X8 (100-200#) onto a column followed by cleaning washes to remove potential interfering elements in the resin. Separation of the HSE involved a concentrated HNO₃ elution, which collected the majority of Ir, Re, Pt, and Ru, and a concentrated HCl elution, which collected the majority of Pd. These HSE were measured using a *Cetac Aridus II* desolvating nebulizer coupled to the *ThermoScientific* iCap q ICP-MS. Rhenium, Ir, Pt, Pd, and Ru isotopic ratios measured were corrected for mass fractionation within the machine, using the deviation of the standard average run on the day of analysis relative to the natural ratio of the element. The total procedural blanks had $^{187}\text{Os}/^{188}\text{Os} = 0.170 \pm 0.006$, with quantities (in picograms) of 2.8 ± 3.59 [Re], 13.4 ± 7.35 [Pd], 1.46 ± 0.92 [Pt], 14.3 ± 4.5 [Ru], 2.0 ± 0.86 [Ir] and 0.9 ± 0.36 [Os] (n = 2; all errors are 1SD). Blanks from the analytical campaign led to negligible corrections to samples (<2%). Concentrations and isotopic compositions for total analytical blanks are provided in Table 4.

2.5. Analytical development for gold measurements

Laser ablation ICP-MS is an application widely used to characterize the composition of geological samples, however it has had a short-lived history for *in-situ* applications of electrum. In-house reference materials metal standards, Hoba, Filomena, and Coahuila were measured by solution ICP-MS to obtain precise major-, minor, and trace- element concentrations followed by N-TIMS analysis of Os isotopes. Values obtained from our in-house standards were used for the standardization of HSE abundances obtained from laser ablation ICP-MS analysis of electrum to ensure the accuracy and precision of our measurements. Compared to reported values from the literature (Cook et al., 2004; Petaev and Jacobsen, 2004; Walker et al. 2008), our preferred values show subtle differences, and also provide a fuller suite of measurements for elements not previously reported (Table 5). A detailed report of our results, and additional applications, were published in Day et al., (2018) and is included as a supplement in this thesis.

A second phase in the method development process was to improve electrum analysis by LA-ICP-MS. For this purpose, a JM Reef sulfide from the Stillwater Intrusion was analyzed via solution ICP-MS in an effort to create a sulfide internal standard with sufficiently high levels (ppm) of the HSE, as an alternative to USGS metal sulfide reference material MASS-1. A homogenous material is preferred for an internal standard. Coupled with laser ablation raster analysis, the ablation spectra showed that the selected sulfide had multiple sulfide phases due to exsolution and fractionation; phases including pyrrhotite (high in S-Fe), pentlandite (high in Fe-Ni), and chalcopyrite (high in Fe-Cu) (Figure 4). Standardization was performed using iron meteorite in-house standards, Hoba and iron meteorite standards, Filomena and Coahuila, which gave precisions better than 7% (RSD) for all elements listed excluding Au (Table 6). Despite our efforts, the heterogeneity observed in the selected sulfide sample proved unfit for an internal standard. Overall, the results from this work highlights an important issue for analysis of gold samples and prompts future work for method development of sulfide reference material. This work has prompted evaluation of further JM-Reef sulfides, and a single sulfide has now been identified with the requisite properties for a good, homogeneous internal sulfide standard (M. Paquet and R. Hattingh, pers. comm.).

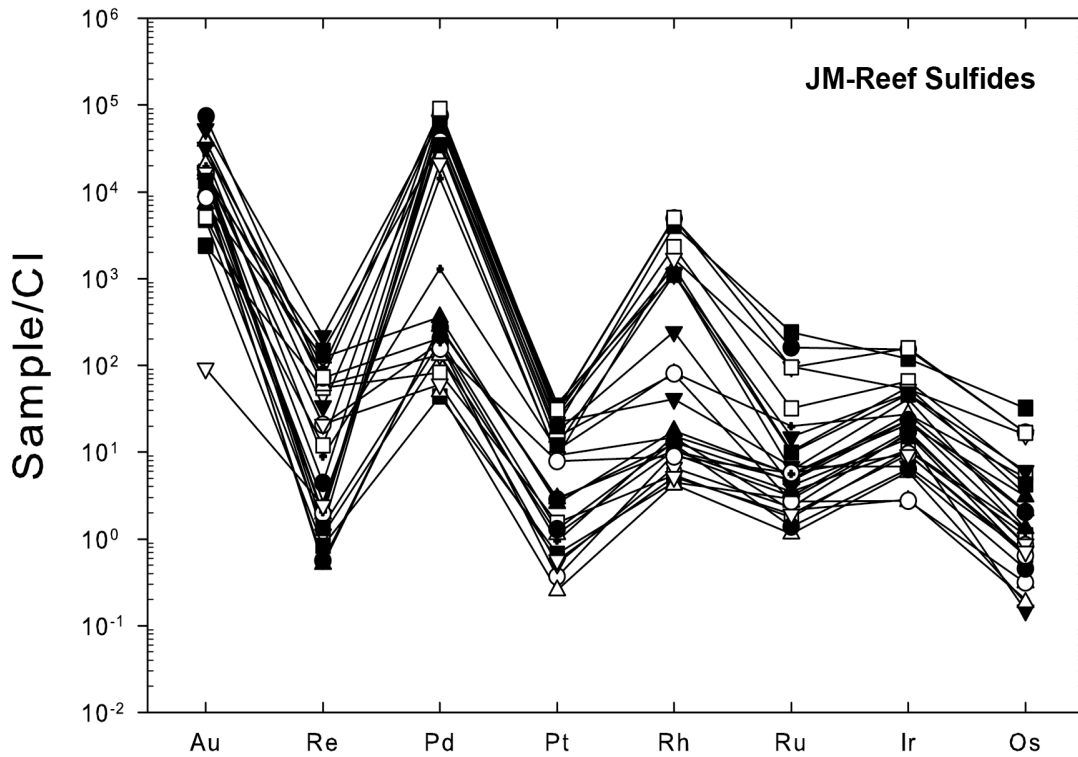


Figure 4: JM-Reef sulfide spectra from LA-ICP-MS analysis plotted as a function of increasing compatibility of HSE, from gold to osmium, versus sample normalized to chondrite. Variable element compositions are due to ablation of multiple sulfide phases. Normalization values are from McDonough & Sun (1995).

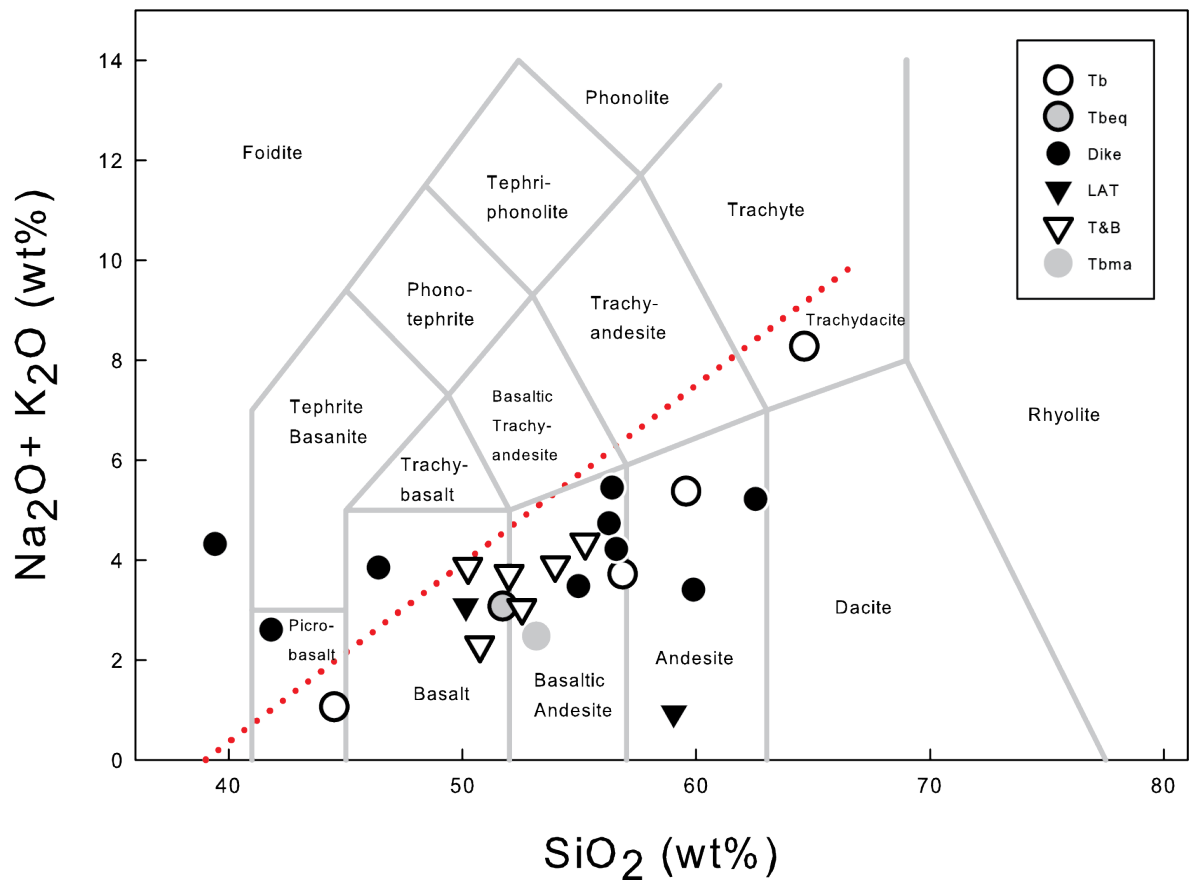
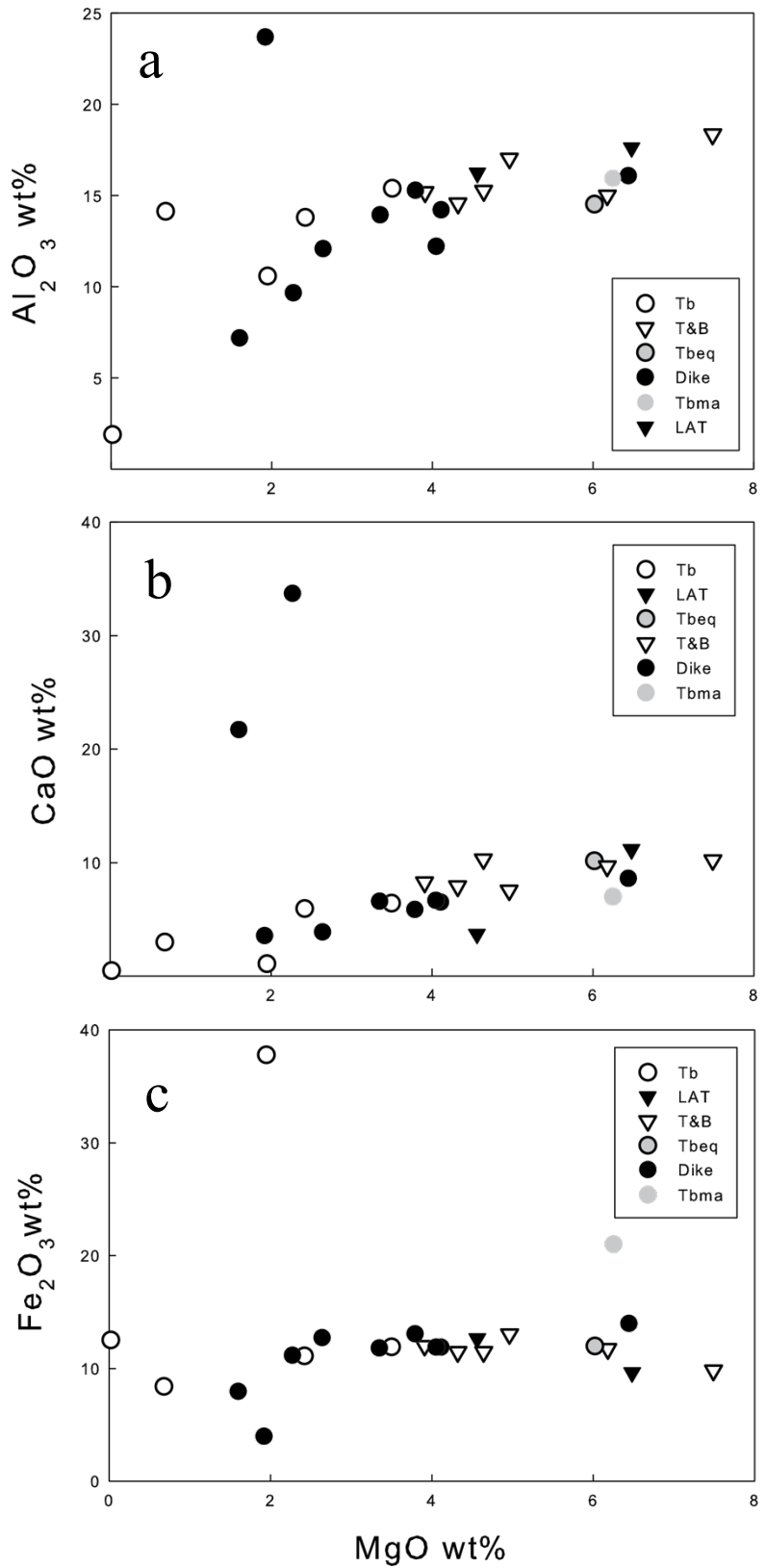


Figure 5: Total Alkalis versus silica (TAS) diagram of the Fire Creek Mine volcanic rocks in Lander County, NV. The diagram displays a range of volcanic compositions with basalt units and dike (circles) and tuff units (triangles) extending from 35 wt% to 70 wt% SiO_2 . Sample 1102-A (composed of 83.5 wt% SiO_2 and 0.32 wt% $\text{Na}_2\text{O} + \text{K}_2\text{O}$) is not included. The red line divides alkalic and sub-alkalic rocks.

Figure 6: MgO versus major element oxide 'Harker' diagrams for basalt units and dike (circles) and tuff units (triangles) at the Fire Creek Mine. Plot (a) and (b) shows increasing Al_2O_3 and CaO with increasing MgO, with no change observed in (c).



3. Results

3.1. Results for Fire Creek country rocks

3.1.1. Whole-rock major- and trace- element concentrations

Country rocks analyzed from the Fire Creek represent the compositional variations of bimodal sub-alkali volcanic rocks observed in the area. These include basalt, basalt-andesite, andesite, trachydacite and a few strongly altered basalt rocks (49-5-1, Tb-3; Figure 5). Tb1 is a trachydacitic unit and it is unique because it is the only unit that postdates mineralization. Major element compositions of Fire Creek rocks generally exhibit a positive trending slope when plotting Al_2O_3 , Fe_2O_3 , and CaO (wt. %) against MgO (wt. %) (Figure 6). The majority of the samples have <1.60 to 7 wt. % MgO, with the exception of samples 1102-A and 1106 (<1 wt.%) and 427-6 (7.49 wt. %). Loss on ignition for the basalt rocks ranges from 0.53-15.7 wt. %, with the exception of sample 702-1 (21.8 wt. % LOI), and tuff rocks range from 3.5-7.4 wt. %, with the exception of heavily altered sample LAT (1108) at 22.1 wt. % (Table 3). Large variation in dike composition implies multiple diking events with mafic and andesitic dikes both present at the Fire Creek location.

New trace-element abundance data highlight the bimodal origin of the volcanic sequence at the Fire Creek. There is a clear distinction in both trace element abundances and rare earth element abundances (REE) in the dike samples, as well as other country rocks (Figure 7, 8). The upper basalt units display variable compositions. Two samples from the upper basalt units (1104 and 1109) display identical concentrations of incompatible trace elements, with Rb being slightly depleted in one of them, and in the REE (Figure 7a, 7b). In contrast, upper basalt units 1102-A and 1102-B have significantly different incompatible trace elements and REE compositions. Trachydacitic sample 1106 is significantly enriched in all elements, except for Sr and Ti, compared to the rest of the suite. The lower basalt group is composed of two samples that are slightly depleted relative to the upper basalt units 1104 and 1109. Dike samples overall are enriched in more incompatible trace elements relative to less incompatible (REE) (Figure 8a). The dike samples have broadly similar enrichments and depletions, except for elevated enrichments in Pb, which can be attributed to crustal contamination, and a strong depletion in Sr, due to alteration, in sample 702-1. The upper tuff and lower tuff units discretely display a down

sloping pattern from more incompatible elements to least incompatible elements. Slight variations in upper tuff sample 427-6 shows a strong depletion in Pb while lower tuff sample 1108 is slightly enriched in Th and depleted in Sr compared to the remaining elements. While some effect can be expected from hydrothermal alteration observed in these samples (cf., high U and Sr), the compositional variability among the units is most readily attributed to partial melting source processes and crustal assimilation.

Country rocks and dikes, display both small negative and positive europium anomalies ($[Eu^*]_N = 0.87$ to 1.54 , where $Eu^* = Eu_N / (\sqrt{Sm_N * Yb_N})$, and N denotes normalization to primitive mantle), with sample FC 47-1-2 displaying the lowest negative anomaly of the suite. All samples display similar negative anomalies for Nb ($[Nb^*]_N = 0.27-0.59$, where $Nb^* = Nb_N / (\sqrt{Th_N * La_N})$) and Zr ($[Zr^*]_N = 0.65$ to 0.91), with the exception of basalt sample FC 1106 ($[Zr^*]_N = 1.01$), which is the trachydacitic cap rock that postdates mineralization at the Fire Creek Mine. Basalt units FC 1102-A and 1102-B display significantly large positive europium anomalies ($[Eu^*]_N = 1.4$ and 1.5) relative to the rest of the suite of basalt units analyzed which have an europium anomaly that is <1 and low negative zircon anomalies ($[Zr^*]_N = 0.65$ and 0.68 , respectively) relative to the large negative anomalies observed in the rest of the sample suite ($[Zr^*]_N = 0.80$ to 0.91).

Hydrothermal alteration is particularly distinct in the REE compositions highlighting fluid mobile incompatible elements (Figure 7b, 8b). The tuff units show a generally decreasing concave up-sloping primitive mantle REE pattern. Basalt rocks with distinct alteration (samples 1102-A and 1102-B) are enriched in the light REE (e.g., La, Ce) relative to the other basalt units at the Fire Creek (Figure 8b). Upper tuff units 1108 and 427-1 and lower tuff unit, 427-6 also display similar mobile behavior relative to the rest of the tuff units, thus setting them apart. Alteration is particularly evident when plotting La/Yb and La/Sm ratios (Figure 9). Here, FC 1102 (-A and -B) samples both lie far from the rest of the rocks which show consistent increasing relative abundances of the REE with primitive mantle-normalized La/Yb ratios. Sample 1102-A indicates a La/Yb of 5.23 and La/Sm of 1.22 compared to a higher La/Yb ($[La/Yb]_N = 16.019$) and La/Sm ($[La/Yb]_N = 2.079$) in whole rock 1102-B.

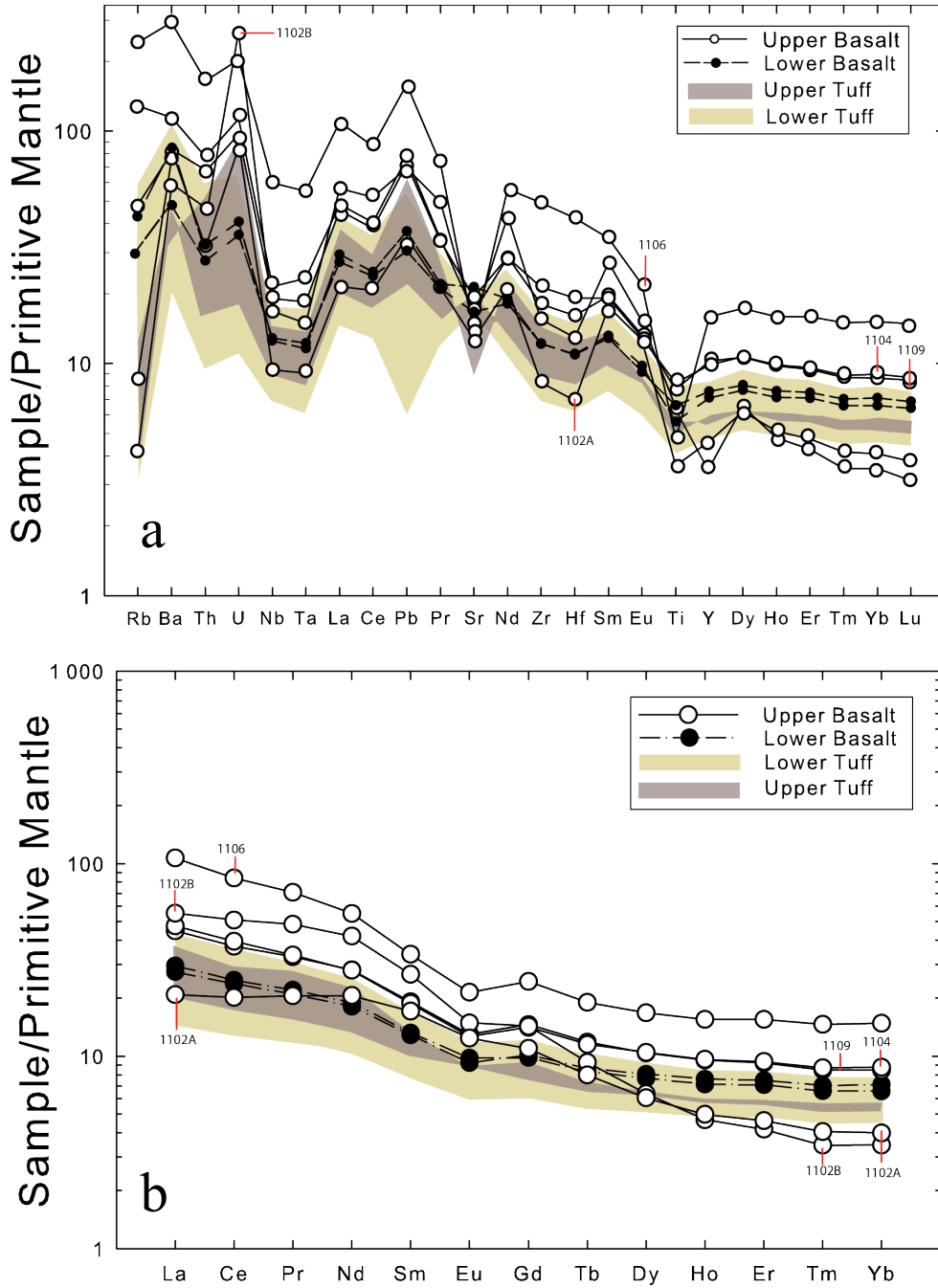


Figure 7: Trace element geochemistry of the Fire Creek country rocks as (a) primitive mantle normalized incompatible trace element abundances and (b) primitive mantle normalized rare earth element abundances versus upper basalt, lower basalt, upper tuff, and lower tuff. Primitive mantle normalization from McDonough & Sun (1995).

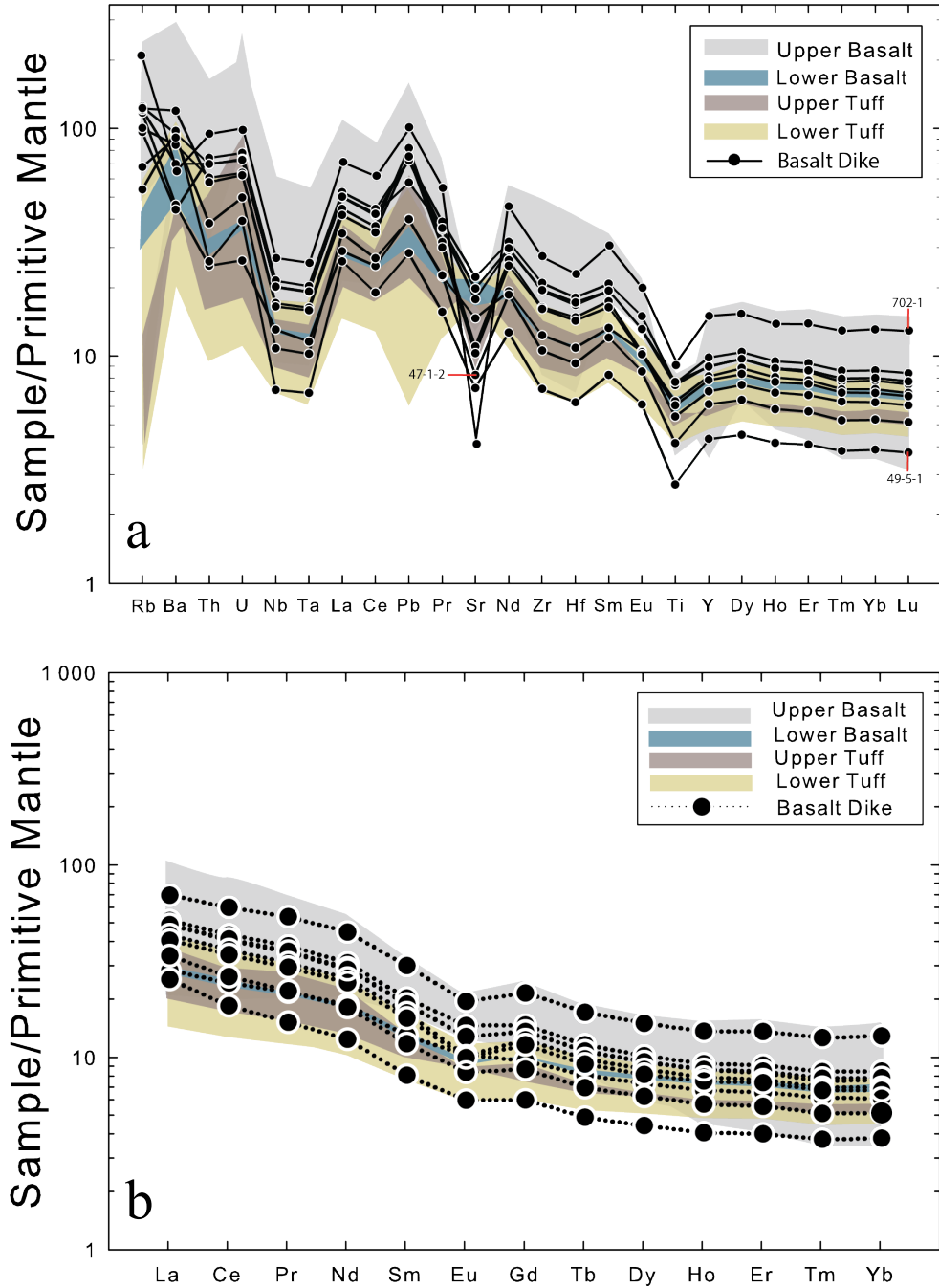


Figure 8: Trace element geochemistry of the Fire Creek country rocks (shaded polygons) versus dike as (a) primitive mantle normalized incompatible trace element abundances and (b) primitive mantle normalized incompatible rare earth element abundances versus upper basalt, lower basalt, upper tuff, and lower tuff units. Primitive mantle normalization from McDonough & Sun (1995).

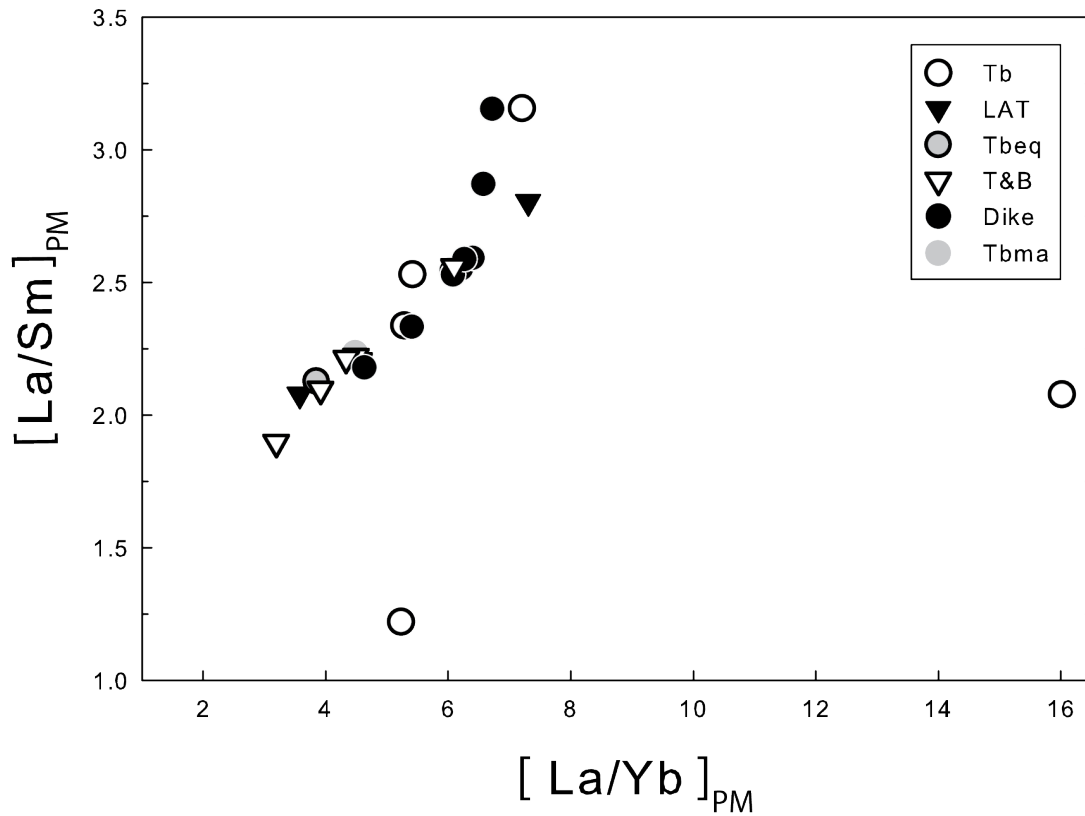


Figure 9: Lanthanum/Samarium versus lanthanum/Ytterbium for basalt units and dike (circles) and tuff units (triangles) of the Fire Creek electrum-host rocks. Fire Creek host rocks display ratios near unity ($R^2= 0.8624$) except for samples 1102-A and 1102-B suggesting a different source for these samples. Ratios are normalized to primitive McDonough & Sun (1995).

3.1.2. Highly siderophile element abundances

Absolute and relative abundances of the highly siderophile elements (HSE: Os, Ir, Ru, Pt, Pd, Re) for electrum and country rock aliquots are reported in Table 7. Country rocks spanning the range of MgO (4.3 to 7.5 wt. %) contents were selected, and electrum was extracted from the vein host. The HSE show systematic variation, for both host-rocks and electrum (Figure 10, 13). Country rocks are relatively depleted in HSE abundances compared to electrum, with highly depleted concentrations in Pt and Ir relative to Ru and Os. Country rocks analyzed have Pd concentrations ranging from 1.28 to 12.8 ppb and Re concentrations ranging from 0.97 to 2.7 ppb. Country rock samples exhibit similar concentrations for Pd, with the exception of samples 427-1, 427-6, and 427-2 which have significantly lower Pd (<0.011 ppb) than the remaining suite. Likely, very similar Ru and Pt abundances can be observed in all samples, but range in Ir/Ru with all samples showing <0.07 , except for FC 47-1-2 ($[\text{Ir}/\text{Ru}]_{\text{N}} = 0.54$), 702-3 ($[\text{Ir}/\text{Ru}]_{\text{N}} = 0.21$), and 427-7 ($[\text{Ir}/\text{Ru}]_{\text{N}} = 0.45$).

3.1.3. ^{187}Re - ^{187}Os isotope systematics of host rocks

Osmium isotope ratios for host-rocks are reported in Table 7. The $^{187}\text{Os}/^{188}\text{Os}$ for whole rock samples range from 0.3384 to 1.782, with basalt sample FC 47-1-2 ($^{187}\text{Os}/^{188}\text{Os} = 1.219 \pm 0.003$) and 472-2 ($^{187}\text{Os}/^{188}\text{Os} = 1.782 \pm 0.002$) possessing more radiogenic $^{187}\text{Os}/^{188}\text{Os}$ than the rest of the sampled rocks. The tuff units analyzed have $^{187}\text{Re}/^{188}\text{Os}$ values in a close range from 22 to 122, while basalt units display a wide range from 0 to ~ 5000 . In fact, tuff units overall possess less radiogenic $^{187}\text{Os}/^{188}\text{Os}$ (0.3384 to 0.9141) relative to basalt units analyzed. The Re-Os isotope compositions of all host-rocks do not plot near the 15.9 Ma primitive mantle evolution line (Figure 11). Removing the most radiogenic samples (FC 47-1-2; 427-7), with relative unsupported ^{187}Os (from Re loss), yields an error-chron with an $^{187}\text{Os}/^{188}\text{Os}$ initial of 0.4965.

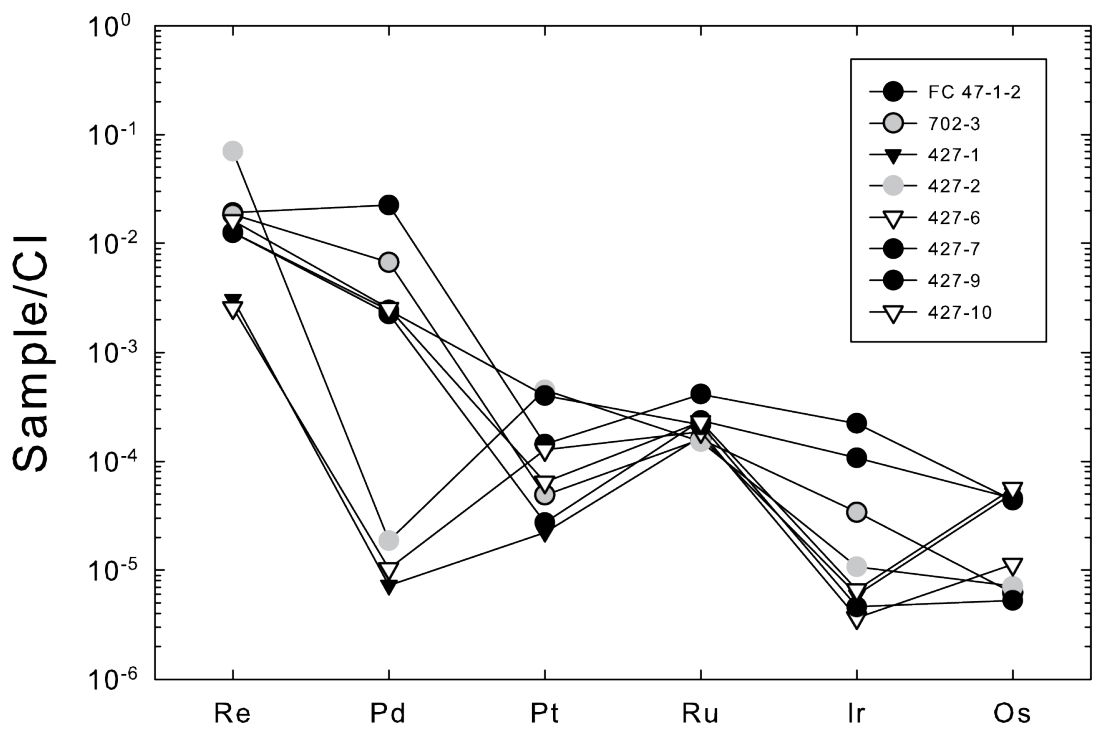


Figure 10: Chondrite normalized highly siderophile element patterns for Fire Creek host rocks for basalt units and dike (circles), and tuff units (triangles) from incompatible Re to compatible Os. Data for 427-2, 427-6, and 427-1 have the most fractionated Pd concentrations. Normalization values are from Day et al. (2016).

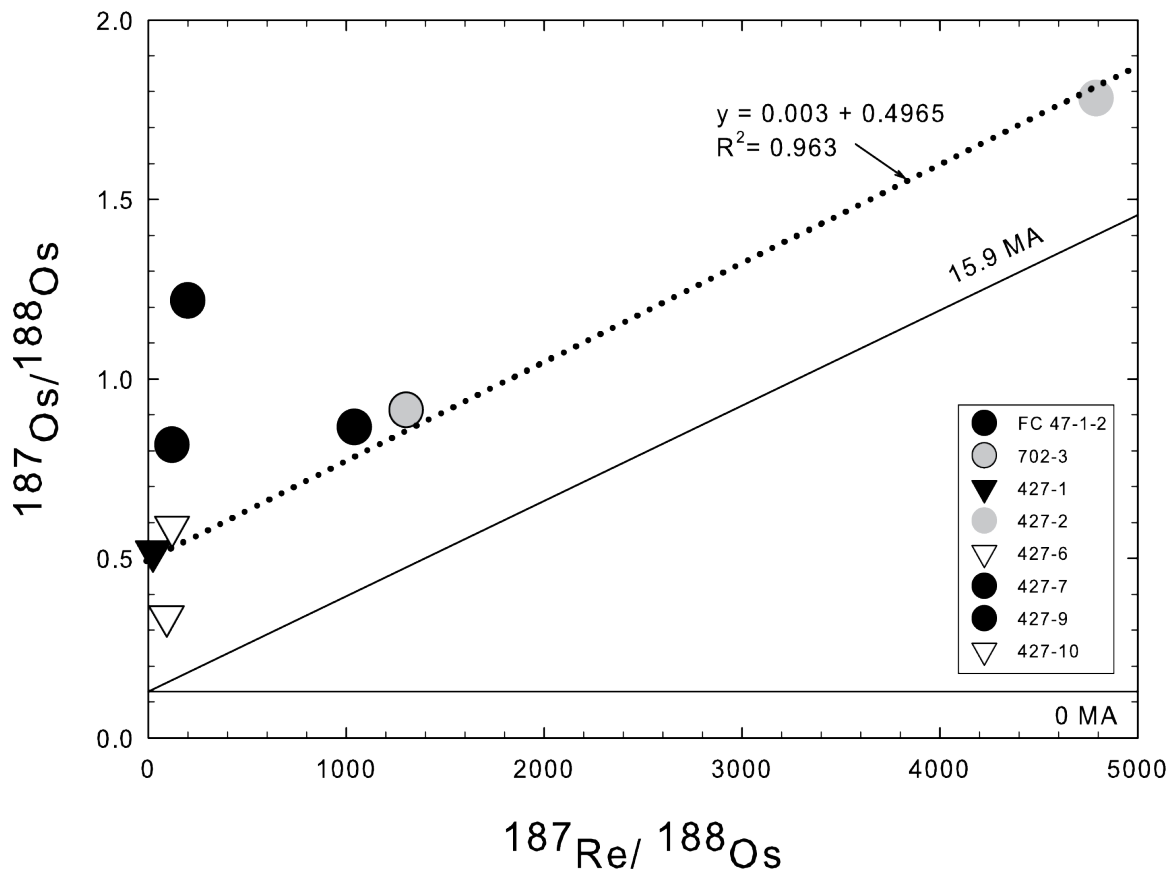


Figure 11: $^{187}\text{Re} - ^{188}\text{Os}$ versus $^{187}\text{Os} - ^{188}\text{Os}$ for Fire Creek electrum with a 0 Ma and 15.9 Ma reference line [$^{187}\text{Os}/^{188}\text{Os}_i$ for primitive mantle from Meisel et al., 2001] as a solid line and trend line (dotted) with average $^{187}\text{Os}/^{188}\text{Os}_i$ initial of 0.4965 excluding radiogenic FC 47-1-2 and 427-7. Fire Creek host rocks for basalt units and dike (circles), and tuff units (triangles).

3.2. Results for electrum grains

3.2.1. Electrum compositions by LA-ICP-MS

In-situ laser ablation spots for 49 electrum phases analyzed across four samples during the course of this study are summarized in Table 7. Figure 12a displays ablation averages plotted as a function of core for this study and compares them to electrum and sulfide laser analysis previously reported in Perez (2013). Electrum cores typically yielded results below the detection limit for one or more highly siderophile elements, including Re, Pt, Rh, Ru, Ir, and Os resulting in an incomplete suite of HSE data. Here, ablation averages for electrum cores appear to have relative element variability within a core but overall show “saw-tooth” trends that are visible in all electrum samples. HSE correlations between ratios of Re, Pt, Ir, in electrum patterns indicate that sulfide phases exert control over the highly siderophile element fractionation during mineralization despite element variability per spot analysis within electrum cores. Element fractionation, and therefore variation in element concentrations between cores, were previously interpreted to depend on individual vein mineralization and location in the basalt host rock (Perez, 2013).

The HSE averages measured in core 5 for a single grain share similar characteristics to those observed in this study, with the exception of an increased concentration in Pd and decreased concentration of Pt in cores 1 and 3 (Figure 12a). In particular, cores 1 and 2 appear to have similar interelement partitioning. As previously reported, HSE values for core 5 displayed an antithetical fractionation pattern to that of core 6 (Perez, 2013). A broadly similar antithetical fractionation behavior is observed in electrum analyzed for this study, with the exception of core 3. Results for individual laser ablation spots for all cores are variable (Table 8; Figure 12b). Cores 2 and 3 indicate up to 5 % variability for all elements while variability in cores 1 and 4 are significantly higher. Core 1 shows up to 7% variability in distribution of Re, Pt, Rh, Ru, Ir, and Os with the exception of Pd (69%) while core 4 indicates a high variability in distribution between 18 to 28% with the exception of Ru, Rh, and Os (up to 2%). Core 5 and 6 generally show a variability better than 14% with the exception of Re (54%) in core 6.

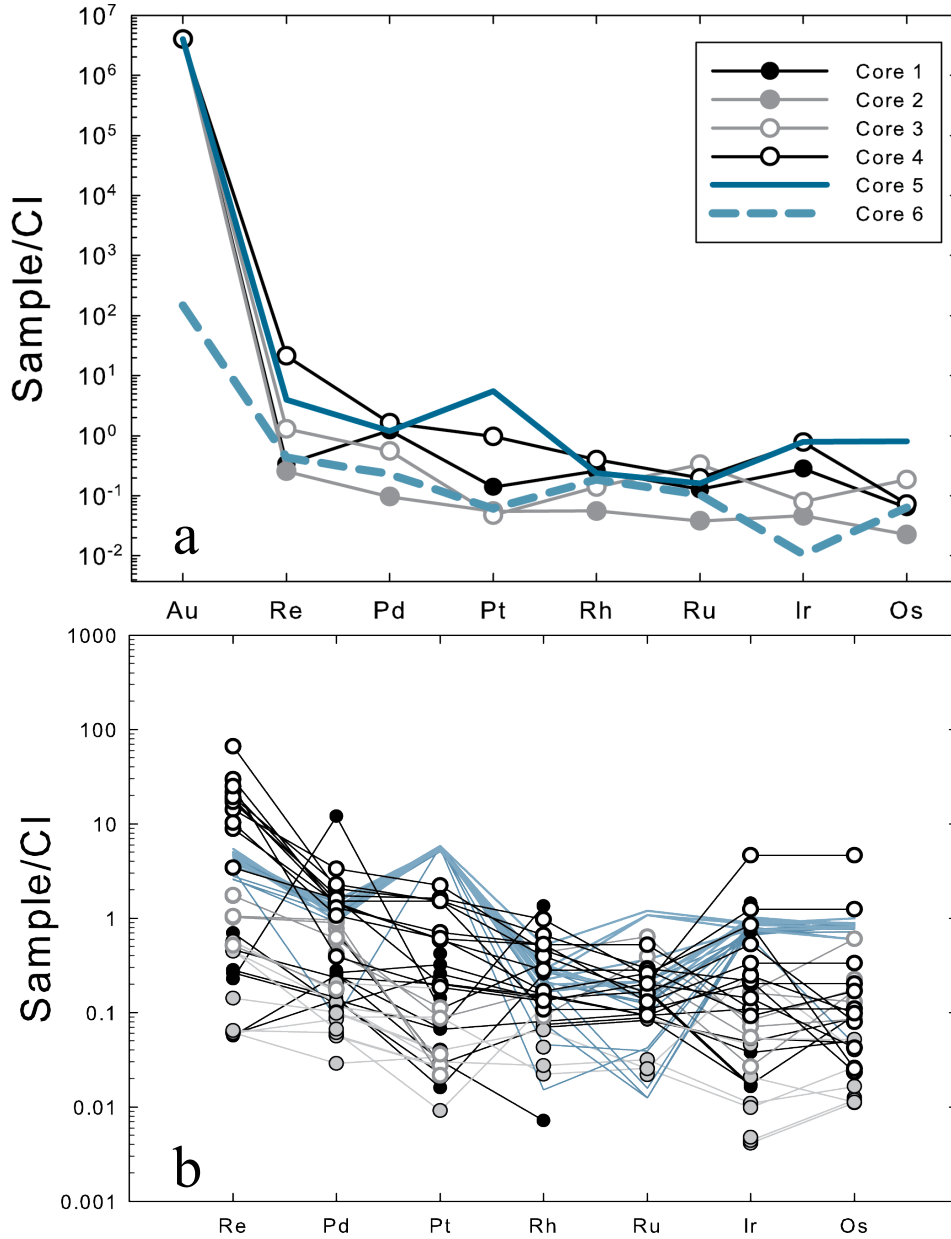


Figure 12: Laser ablation ICP-MS analysis for Core 1 (FC 50 1-2-2), Core 2 (FC 50-1-3-1), Core 3 (FC 50-1-3-2), and Core 4 (FC 50-2-1) of electrum were obtained at the Scripps Isotope Geochemistry Laboratory. Each core represents a sample and multiple electrum grains were targeted for spot analysis within a sample. Laser ablation data of Core 5 for a single electrum grain in FC 50 1-2-2 and Core 6 for a sulfide that mineralized simultaneously, are from Perez, (2013). Highly siderophile element patterns versus (a) CI-chondrite normalized electrum averages per core and (b) electrum spot analysis normalized to CI-chondrite (Day et al., 2016).

3.2.2. Highly siderophile element abundances

Electrum samples are enriched in the HSE compared to country rocks, and have higher Re, Pd, and Ir concentrations relative to Pd, Ru, and Os (Figure 13). Electrum samples have generally similar abundances compared to the variability observed in the country rocks. Electrum analyzed produced Re (0.031-5.02 ppb), Pd (1.8-23.2 ppb), Pt (14.9-95.7 ppb), Ru (0.85-20.2 ppb), Ir (0.22-6.84 ppb), and Os (0.0091-0.206 ppb) (Table 7). All elements appear to be preferentially fractionated into the electrum samples relative to the rocks. In particular, Re, Pd, and Os normalized concentrations for electrum coincide with Re, Pd, and Os concentrations for the host rocks. The electrum suite shows similar inter-fractionation patterns, with the exception of two samples showing increased concentrations in Pd and Ru compared to the rest of the suite. In general, CI-chondrite-normalized HSE patterns for country rocks and electrum show a “saw-tooth” pattern with enrichments in electrum related to depleted concentrations in the country rocks, similar to the observed laser ablation patterns.

3.2.3. ^{187}Re - ^{187}Os isotope systematics of electrum grains

Isotopic Os ratios for electrum aliquots are reported in Table 7. The $^{187}\text{Os}/^{188}\text{Os}$ for all the electrum analyzed in this study display a range of measured $^{187}\text{Os}/^{188}\text{Os}$ values that lie between 0.2107 to 0.8800, with sample FC 50-2-1 Au III which is even less radiogenic with a $^{187}\text{Os}/^{188}\text{Os}$ initial value ($^{187}\text{Os}/^{188}\text{Os} = 0.1454 \pm 0.002$) (Figure 15). Electrum grains have $^{187}\text{Re}/^{188}\text{Os}$ values that span from 78 to ~3500. Compared to country rock values, electrum analyses display less radiogenic $^{187}\text{Os}/^{188}\text{Os}$. Electrum grain $^{187}\text{Os}/^{188}\text{Os}$ initials display two radiogenic trends, one above the trend line (FC 50-2-1 Au III, FC 50-2-1a, FC 50-1-3-2a, and FC 50-1-3-2b) and the other above the trend line (FC 50-1-3-2, FC 50-1-2, FC 50-2-1b) in Figure 15. Rhenium-Osmium isotope compositions do plot within the 15.9 Ma primitive mantle evolution line and define an error-chron relationship. Combined the electrum yield an $^{187}\text{Os}/^{188}\text{Os}$ initial of 0.1588, implying a strong mantle (0.1296; Meisel et al., 2001), versus a crustal component (~1; Saal et al., 1998).

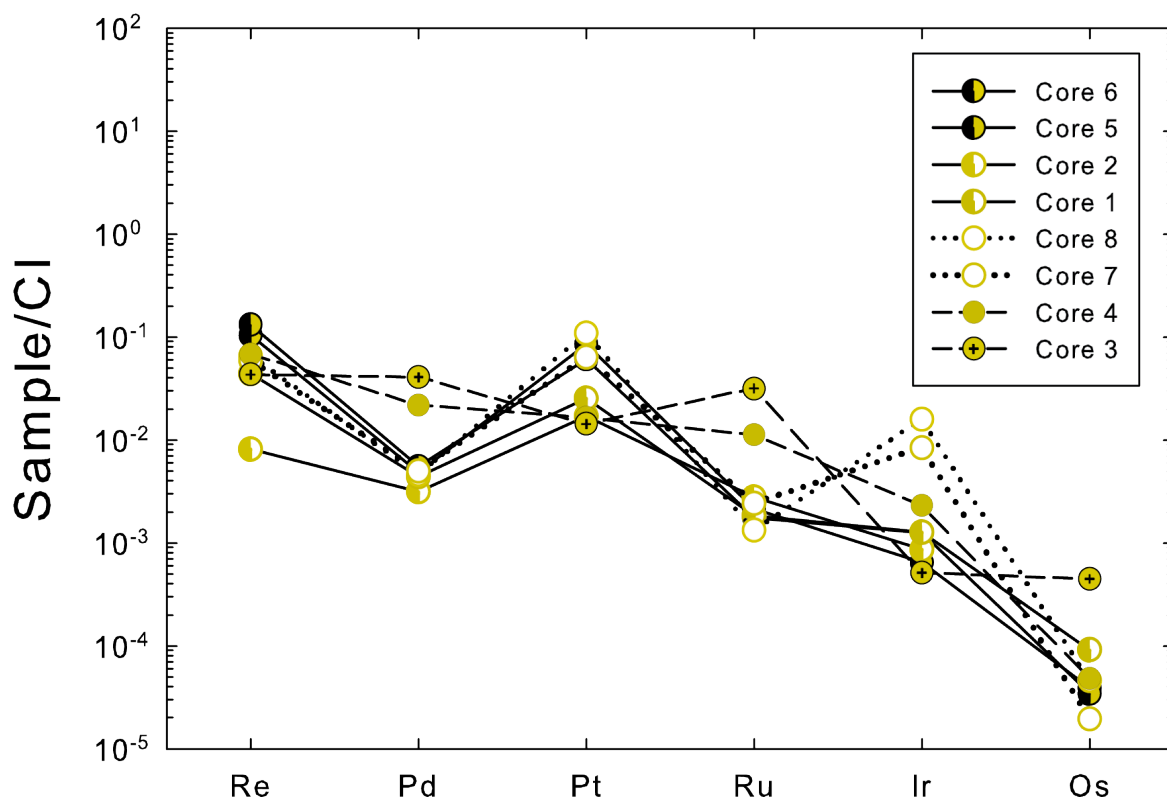


Figure 13: Highly siderophile element patterns of Fire Creek electrum grains from moderately incompatible Re to compatible Os as chondrite normalized abundances versus electrum aliquots analyzed by column chemistry and solution ID ICP-MS. Duplicate symbols (in gold) represent electrum grains sampled from the same vein. Chondrite normalization from McDonough & Sun (1995).

4. Discussion

4.1. Geochemistry and alteration of the host rocks

Low sulfidation Au-Ag epithermal ore at the Fire Creek is dominantly hosted by Mid-Miocene basalt compositions. The majority of dike samples exhibit alteration caused by geothermal processes which likely occurred during a sub-boiling phase during the same process responsible for deposition and pre-concentration of gold and silver (John et al., 2003). An overall trend of alteration is confirmed by the low $\text{Na}_2\text{O}+\text{K}_2\text{O}$ contents in the Fire Creek suite. Samples in this study exhibit high degrees of secondary alteration manifested in the bulk rock data as loss of ignition values up to 22.1 wt. % for the country rocks, and similar LOI values, up to 21.8 wt. % for the dike, which reflect the presence of alteration minerals related to magmatic and hydrothermal alteration during gold mineralization. Trace element abundances can be altered by a variety of geologic process with chemical evidence of hydrothermal alteration in the host rocks at the Fire Creek. Post-emplacement hydrothermal alteration of the host rocks affected relative and absolute abundances of fluid mobile incompatible trace elements (e.g. Rb, Ba, Sr) and the light-REE, but heavy-REE acted as immobile elements. Samples 702-1 and 1108 in particular show elevated concentrations of U, Ba, and Pb which are consistent with alteration effects revealed by high loss on ignition.

New incompatible trace element data for host rocks exhibit trace element concentrations that agree with depletion and enrichment patterns observed in the dike. Concentrations for all basalt, tuff, and dike samples share broadly similar enrichments in Ba, U, Pb, Nd, and Sm and depletions in Nb, Ta, Sr, and Ti. Based on incompatible trace element data, host rocks analyzed share characteristics indicative of the same source host as the dike. Rare earth elements exhibit the same behavior, with elevated LREE elements relative to HREE, negative Eu^* , and constant HREE concentrations for all samples, except for silicic samples 1102-A and 1102-B which have a La/Yb of 5.23 and 16.0 (Figure 9), and a large positive europium anomaly at 1.4 and 1.54 relative to the rest of the suite ($[\text{La}/\text{Yb}]_N < 7.2$; $\text{Eu}^* < 1.1$). Compositional similarities in incompatible trace element features suggest that the sequence of host rocks at the Fire Creek, with the exception of 1102-A and 1102-B, reflect a co-genetic suite of bimodal transitional sub-alkalic rocks.

Ages and similar styles of bimodal volcanism of Au mineral deposits occur in the Northern Nevada Rift. This volcanism and associated mineralization occurred in a relatively narrow time period between 16.5 to 15 Ma, with ore emplacement at the Fire Creek between 16.1 and 15.9 Ma (Millard et al., 2018). These ages indicate that the host rocks were erupted within a relatively narrow time span of ~200 ka by the rifting of the Northern Nevada Rift at the Fire Creek site. Stratigraphy of the host rocks at the Fire Creek must have been emplaced prior to epithermal gold mineralization, followed by the intrusion epithermal gold. This relationship should project a chemical distinction between the units and the dike, as they would be expected to come from a different source host. However, no evidence from the geochemistry of the dike, which intrudes the host rocks, suggests that it formed from a source different to that of the host rock.

Initial Os isotopic values for samples from different host rocks at the Fire Creek exhibit highly radiogenic $^{187}\text{Os}/^{188}\text{Os}$ signatures relative to $^{187}\text{Os}/^{188}\text{Os}$ for the primitive mantle (Figure 11). Samples 47-1-2 and 427-7 in particular are significantly more enriched in ^{187}Os relative to the rest of the suite and have lower ^{187}Re concentrations. Incompatible trace element abundances also possess strong Rb, Nb, Ta, Hf, and Zr depletions across the host rock suite and dike. Incompatible trace element depletions of these elements are trace element signatures typically observed in the continental crust (Weaver and Tarney, 1984; Rudnick and Gao, 2003), thus suggesting a crustal component. Chemical evidence indicates that the Fire Creek host rocks must have seen substantial crustal contamination with addition of Os to influence radiogenic signatures in the host rock suite and explain incompatible trace element depletions.

4.2. Differences and similarities between LA-ICP-MS analyses and isotope dilution

Absolute and relative concentrations of the highly siderophile elements in electrum grains are different between laser ablation ICP-MS and solution ID ICP-MS techniques (Figure 14). Electrum grains measured by laser ablation ICP-MS have consistently higher and flatter patterns compared to patterns obtained by solution ID ICP-MS, with Re, Pd, and Pt that are within a factor of 10, but Os and Ir concentrations that can be quite different (1-3 orders of magnitude). There are two possible causes for this. Impurities in the electrum, as noted previously by Perez (2013), are a possible cause since porous electrum grains are observed throughout the core. It could also be an artifact from analysis (smaller mass from LA vs ID). However, these are not related to impurities for electrum measured by solution ID, as electrum was treated in HCl to remove sulfide.

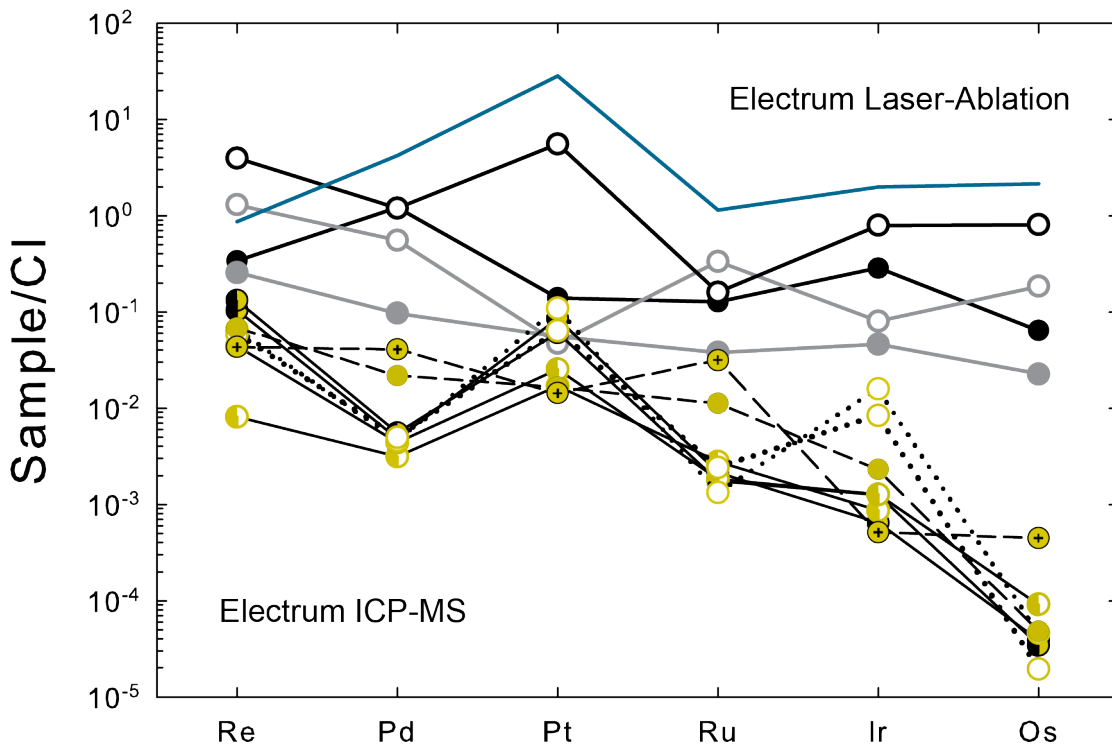


Figure 14: Highly siderophile element patterns of Fire Creek electrum grains from moderately incompatible Re to compatible Os as chondrite normalized abundances versus electrum aliquots analyzed by *in-situ* laser ablation of electrum cores compared to solution ID ICP-MS. Duplicate symbols (in gold) represent electrum grains sampled from the same vein. Laser ablation core refer to Figure 12. Chondrite normalization from McDonough & Sun (1995).

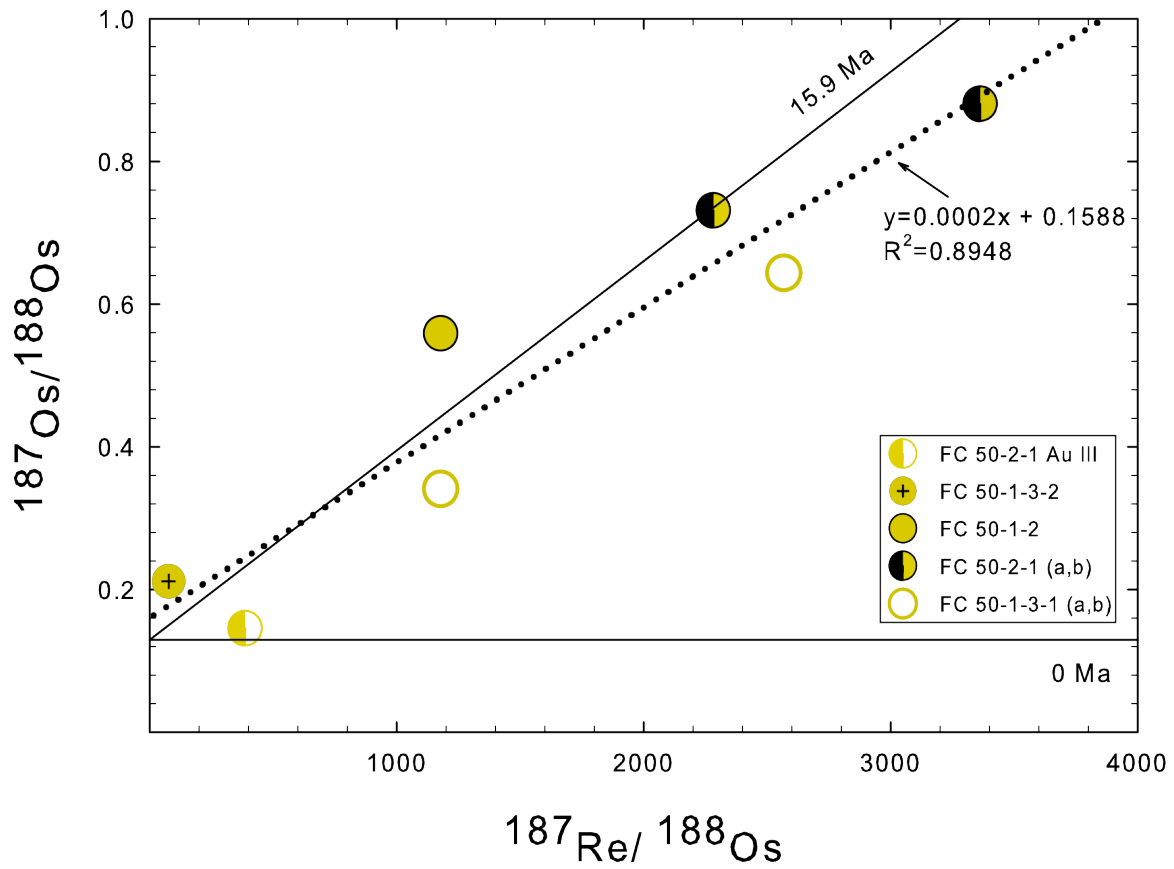


Figure 15: $^{187}\text{Re}-^{188}\text{Os}$ versus $^{187}\text{Os}-^{188}\text{Os}$ for Fire Creek electrum with a 0 Ma and 15.9 Ma reference line [$^{187}\text{Os}/^{188}\text{Os}_i$ for primitive mantle from Meisel et al., 2001] as a solid line and trend line (dotted) with average $^{187}\text{Os}/^{188}\text{Os}$ initial of 0.1588. Duplicate symbols (in gold) represent electrum grains sampled from the same vein.

4.3. Crustal contamination and relation to the Columbia River flood basalts

In addition to the incompatible trace elements that effectively argue for crustal contamination of host rocks, the radiogenic Os isotopic signatures observed in the Fire Creek rocks can only be attributed to contamination of the primary magma by crustal material with radiogenic $^{187}\text{Os}/^{188}\text{Os}$. Studies on the Columbia River flood basalts have documented geochemical variations in Sr, Nd, Os and Pb isotopes that are consistent with crustal contamination of mafic mantle-derived magmas (e.g., Chesley and Ruiz, 1998; Day et al., 2013). In addition to the Fire Creek being spatially and temporally related to the Columbia River flood basalts (CRFB), it has previously been genetically linked to the CRFB on the basis of Pb isotopes (Kamenov et al., 2007). Unlike incompatible trace elements like Pb, however, Os isotope ratios are highly effective tracers of crustal interactions because the difference in the Os isotopic composition between different reservoirs, crust ($^{187}\text{Os}/^{188}\text{Os} = \sim 1$) and primitive mantle ($^{187}\text{Os}/^{188}\text{Os} = 0.1296$; see Day, 2013), are extreme.

A comparison of Re-Os isotope systematics between the Fire Creek host rocks and the younger dikes and flows (~ 17 -6 Ma) from the CRFB, such as the Imnaha, Wannapum, and Grande Ronde formations (Figure 2), suggest that they experienced similar extents of assimilation and fractional crystallization through their emplacement (Chesley and Ruiz, 1998; Vye-Brown et al., 2013). There is clear dispersion of samples around the 15.9 Ma age reference line, with the Imnaha Formation exhibiting a primitive radiogenic signature close to the initial $^{187}\text{Os}/^{188}\text{Os}$ for primitive mantle (Figure 16). All CRFB formations generally agree with the age reference line and display variable enrichments in ^{187}Os . For example, the Imnaha and Wannapum Formations have $^{187}\text{Os}/^{188}\text{Os}_i$ values that range from ~ 0.1344 to 3.047 and $^{187}\text{Re}/^{188}\text{Os}$ values up to ~ 5000 . Using the host rocks Re-Os isotope systematics to estimate an age of formation for the Fire Creek yield ~ 14.1 Ma, which is ~ 2 Ma younger well than the age measured from $^{40}\text{Ar}/^{39}\text{Ar}$ dating of adularia bands. These observations establish evidence for a genetic association between the Fire Creek host rocks and the Columbia River Basalt Group, in addition to incompatible trace element depletions, but also suggests that the host rocks' elevated radiogenic signatures are attributed to contamination from a crustal component enriched in ^{187}Os , as observed in the CRFB.

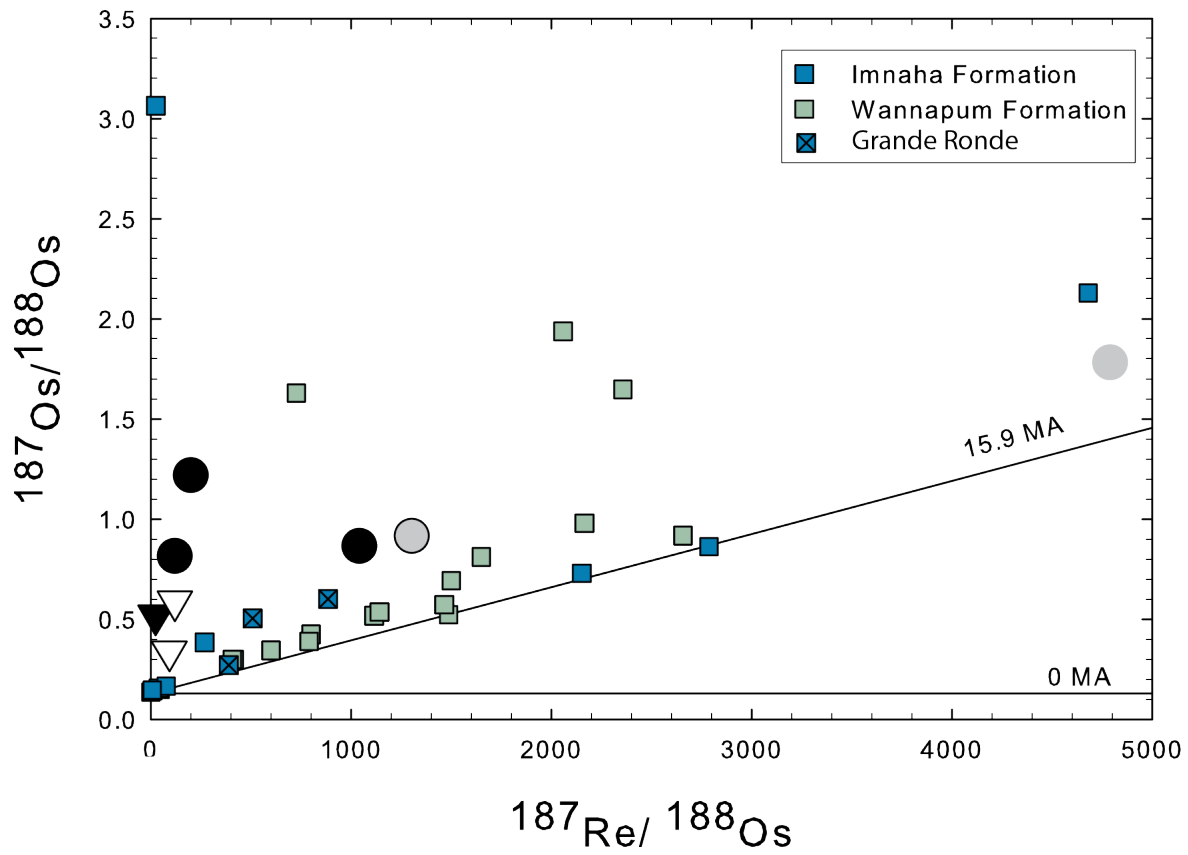


Figure 16: ^{188}Os versus $^{187}\text{Os} - ^{188}\text{Os}$ for Fire Creek electrum and Columbia River Basalt Formations with a 0 Ma and 15.9 Ma reference line [$^{187}\text{Os}/^{188}\text{Os}_i$ for primitive mantle is from Meisel et al., 2001] as a solid line. Fire Creek host rocks for basalt units and dike (circles), and tuff units (triangles). Data for Imnaha and Grande Ronde are from Chelsey et al. (1998) and data for Wannapum are from Vye Brown et al. (2013).

4.4. Source of electrum and implications for ore genesis

The geochemical nature of host rocks and electrum in the Northern Nevada Rift have not generally been discussed in studies of gold mineralization, with only a few studies directed at understanding the source of the gold (Hofstra and Creaser, 2009; Saunders et al., 2008). Rhenium and the platinum-group elements (PGE: Os, Ir, Ru, Rh, Pt, and Pd) are powerful geochemical tools, because of their intimate relationship to Au, that display distinct partitioning behavior between highly compatible Os, Ir, Ru and Rh relative to compatible Pt and Pd, and moderately incompatible Re and Au during melting and crystallization (Day, 2013). Inter-element fractionations can provide resolution to the processes that control sulfur or alloy formation and source (Perez, 2013). In this study, characterization of bulk samples and thin sections of electrum grains was made possible using *in-situ* laser ablation. Data display near chondritic HSE concentrations and agree with antithetical fractionation patterns to sulfide (core 6) as described for a single electrum grain in Perez (2013) (Figure 12a, 12b). Core 6 displays a strong depletion in Pd, Rh, and Ru with elevated Ir and Os, highlighting the compositional variability within one electrum grain (Figure 12b). While some elements appear to have a similar partition coefficients, further analysis of electrum suggests that there is different partitioning across mineralized ore veins. Characterization of electrum grains via laser ablation provided a first order quantitative measurement of highly siderophile element concentrations key for high precision isotope dilution measurements.

Highly siderophile element abundances and the long-lived ^{187}Re - ^{187}Os system (^{187}Re half-life ~ 42 Ga; Day et al., 2016) are essential tools for understanding processes that are not revealed from other isotope systems due to the affinity of these elements into sulfides and metal alloys. Electrum aliquots analyzed by solution ICP-MS exhibit a clear saw-tooth pattern with decreasing concentrations from moderately incompatible Re to highly compatible Os (Figure 13). With the exception of cores 3 and 4, which contain higher concentrations of Pd, Ru, and Os, all cores display identical saw-tooth depletion trends with high Re concentrations and depleted Os concentrations relative to chondrite. Element concentrations obtained by solution-based ICP-MS analysis agree with inter-element partitioning observed using *in situ* laser ablation and variable fractionation in all cores (Figure 13, 14). The expression of this relationship is particularly clear when I focus on isotope dilution HSE concentrations as they display a systematic fractionation

for whole electrum grains and host rocks. Highly siderophile element concentrations of electrum relative to the host rocks display an antithetical relationship (Figure 10, 13). The electrum grains display negative HSE pattern, with host rocks significantly fractionated below chondritic values and electrum more enriched with near chondritic values. Host rocks largely resemble MORB highly siderophile element concentrations (Day, 2013). Electrum possess elevated Re, Pt, and Ir while the host rocks exhibit lower concentrations of the same element, with the same observed for lower Pd, Ru, and Os. Host rocks preserve lower element concentrations relative to chondrite for all basalt rocks, except for 427-2, tuffs 427-6 and 427-1 which are highly fractionated in Pd. Electrum preserve enriched concentrations despite variable fractionation. The overall trend in electrum HSE abundances resemble that of a fractionated basalt and suggest that HSE partitioning is derived from the basalt its self and, therefore, a magmatic source. Highly siderophile concentrations prove that significant Re/Os fractionation is possible in order to directly date the age of electrum and potentially identify provenance.

The Re-Os system provides evidence for a mantle source of gold in the Northern Nevada Rift. Although incompatible trace element data and Os isotopes for the Fire Creek country rocks suggest a crustal source, the emplacement of gold ore originates from a predominantly mantle component with a $^{187}\text{Os}/^{188}\text{Os}$ initial average composition of 0.1588 for the electrum (Figure 15). A previous study using Pb isotope ratios in gold ores from deposits in the NNR, including Sleeper, Jumbo, Seven troughs and National deposits, attempted to chemically link a mantle source related to the arrival of the Yellowstone hotspot (Kamenov et al., 2007). Lead isotope ratios were compared to multiple flows from the CRFB, including Wannapum and Imnaha, but proved most isotopically similar to Grande Ronde suggesting origin from an isotopically similar source (Kamenov et al., 2007). However, observed isotopic lead compositions for gangue minerals differed to the gold that they hosted and were consistent with leaching of major elements from metasedimentary rocks, proposing that the lead signature, and by association gold, exsolved from mafic magmas at depth which triggered the formation of host rhyolites by crustal melting.

Work by Saunders et al. (2010), utilizing a combined geochemical approach with Pb and Re-Os isotope analysis of electrum samples from Sleeper, Seven Troughs, Tenmile, and Round Mountain (Oligocene), reported an $^{187}\text{Os}/^{188}\text{Os}$ initial of 0.344 ± 0.010 for a single sample from

the Sleeper deposit. The study concluded that their calculated initial Os isotope ratio and Pb isotope data is most coeval with Grande Ronde, however most of their aliquot yielded low Os concentrations (<ppt) proving unreliable at best (Saunders et al., 2010; Kamenov et al., 2007). Rhenium-Osmium isotope data from Saunders et al., 2010 display low Os concentrations for electrum from five different sample sites thus lacking the necessary sample set to obtain isotope systematics that would yield an $^{187}\text{Os}/^{188}\text{Os}$ initial. I suggest that with additional sampling of high grade ore from a focused location studied by Saunders et al. (2010) would likely produce Re-Os isotope systematics similar to those observed for the Fire Creek in this study.

The $^{187}\text{Re}/^{188}\text{Os}$ - $^{187}\text{Os}/^{188}\text{Os}$ systematics for electrum from the Fire Creek Deposit expose a direct link to a mantle source (Figure 15). The electrum yield an average trend line with an initial near the isotopic initial for the 15.9 Ma primitive mantle reference line (0.1588). In the case that the original material for the electrum pointed to uniform initial $^{187}\text{Os}/^{188}\text{Os}$ ratios, the suite would be homogenous and yield an isochronous line pointing to a primitive mantle source. However, the differences in radiogenic ^{187}Os indicate that initial isotopic heterogeneity in the Fire Creek must be inherent and related to emplacement of ore in different veins. This suggests that Os isotope concentrations in electrum must be inherited from host veins, which have slightly variable compositions, such that isotopic ratios acquired at the time of mineralization evolve different radiogenic trends with time (Figure 17a). Isotopic heterogeneity observed in electrum demonstrate that the electrum is primarily coming from a mantle source and a fraction of elevated ^{187}Os is being inherited from a crustal source.

The host rock sample suite is not isochronous therefore indicating some of the samples experienced Re loss or Os addition. This change in Re-Os isotopic ratios is observed in samples 47-1-2 and 427-7. Alteration associated with hydrothermal fluids can account for large degrees of alteration and mineralization and drive relative ^{187}Re loss (Figure 17b). Rhenium loss, as opposed to Os addition, is supported by low Os concentrations (Figure 10). A simple two component mixing calculation demonstrates that the mid- Miocene host rocks in the Northern Nevada Rift must have seen at least 35% crustal contamination. An estimated crustal contamination for electrum resolves that ultimately as much as 96% of the gold from the Fire Creek Deposit is derived from a primitive mantle source.

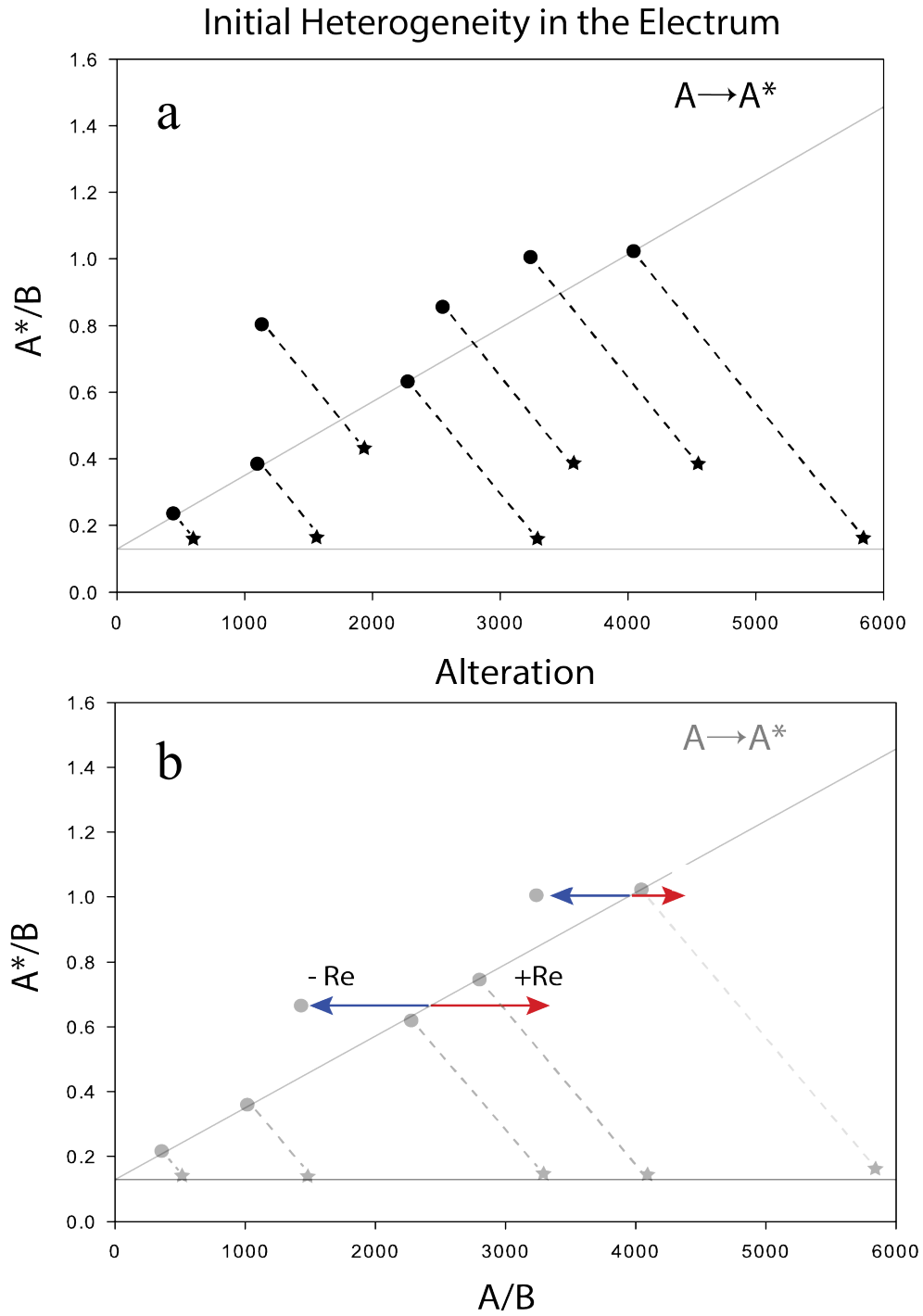


Figure 17: Isotope models demonstrating (a) isotopic heterogeneity due to mixing from different sources and (b) alteration by Re loss or addition in Re-Os isotope ratios.

4.5. Age of Electrum

Direct dating of electrum with Re-Os isotope systematics yields an age of ~13 Ma. Unpublished $^{40}\text{Ar}/^{39}\text{Ar}$ age data from adularia bands from the Vonnie, Karen, and Hui Wu veins at the Fire Creek suggest that the bonanza vein formation occurred between 16 and 15.9 Ma (Millard et al., 2018). Adularia from an electrum hosting vein at the Mule Canyon Deposit agree well with the $^{40}\text{Ar}/^{39}\text{Ar}$ of the Fire Creek, with an age of 15.33 Ma (John et al., 2001). Our Re-Os isotope analysis from the Fire Creek Host rocks yield a younger age at 14 Ma. Age comparisons posit the possibility that ages are inherent of different sources, where adularia veins are predominantly from crust derived fluids as opposed to bulk rocks which have a strong mantle component.

5. Conclusions

The Northern Great Basin is a unique location that has provided up to 10 percent of the world's gold and 3 percent the world's silver production by means of a variety of deposit types and environmental settings (John et al., 2003a). The Fire Creek Deposit is host to high grade Au-Ag epithermal mineralization derived from a mafic end-member of the bimodal-basalt rhyolite volcanism in the Northern Nevada Rift.

Via chemical analysis with methods from *in-situ* laser ablation to Thermal Ionization Mass-Spectrometry, I have shown that the Fire Creek deposit host rocks show strong evidence of crustal contamination prior to their emplacement, followed by large amount of alteration as a result of ore depositing mechanisms. Incompatible trace-elements with significant fractionations in Nb, Ta, Zr, and Hf, and a Re-Os isotope initial value of $^{187}\text{Os}/^{188}\text{Os}$ at 0.4965 with fractionated HSE concentrations support this conclusion.

Electrum grain analyses indicate a mantle origin for Au-Ag epithermal mineralization in the Northern Nevada Rift. Near primitive mantle Re-Os isotope values prove a direct chemical relation to a primitive mantle source. This conclusion is supported by highly siderophile elements in electrum that appear to be fractionated from the host rocks.

Appendix

Copy of: Day, J.M.D., Maria-Benavides J., McCubbin F.M., Zeigler R.A., 2018. The potential for metal contamination during Apollo lunar sample curation. *Meteoritics and Planetary Science*. <https://doi.org/10.1111/maps.13074>.

I am a co-author of this work and conducted measurements of the standard reference materials Hoba, Filomena and Coahuila, as well as measurement of the curation materials.

References

- Best, M.G., Christiansen, E.H., Deino, A.L., Grommé, C.S., McKee, E.H., and Noble, D.C., 1989. Excursion 3A: Eocene through Miocene volcanism in the Great Basin of the western United States: New Mexico Bureau of Mines and Mineral Resources Memoir, v. 47, p. 91–133.
- Bussey, S.D., 1996. Gold mineralization and associated rhyolitic volcanism at the Hog Ranch District, northwest Nevada. *Proceedings of the International Symposium on the Geology and Ore Deposits of the America Cordillera* (Reno, NV), p.181–210.
- Birck, J.L., Bar Matthieu R., and Capmas, F., 1997. Re-Os isotopic measurements at the femtomole level in natural samples." *Geostandards and Geoanalytical Research*, v. 21.1, p. 19-27.
- Camp, V.E., and Ross, M.E, 2004. Mantle dynamics and genesis of mafic magmatism in the intermontane Pacific Northwest, *Journal of Geophysical Research*, v. 109, B08204.
- Camp, V.E., Pierce, K.L., and Morgan, L.A., 2015. Yellowstone plume trigger for Basin and Range extension, and coeval emplacement of the Nevada–Columbia Basin magmatic belt. *Geosphere*, v. 11, p. 203-225.
- Christiansen, R.L., and Lipman, P.W., 1972. Cenozoic volcanism and plate tectonic evolution of the western United States. II. Late Cenozoic. *Philosophical Transactions of the Royal Society of London*, series A, v. 271, p. 249–284.
- Christiansen, R.L., and Yeats, R.L., 1992. Post-Laramide geology of the U.S. Cordillerian region: in Burchfield, B.C., Lipman, P.W., and Zoback, M.L., eds. *Geology of North America*, v. G-3, *The Cordillerian Orogen: Conterminous U.S.*, p. 261–406. Boulder, CO, Geological Society of America.

- Cohen, A.S., and Waters, F.G., 1996. Separation of osmium from geological materials by solvent extraction for analysis by thermal ionisation mass spectrometry." *Analytica Chimica Acta* , v. 332.2-3, p. 269-275.
- Conrad, J.E., McKee, E.H., Rytuba, J.J., Nash, J.T., Utterback W.C., 1993. Geochronology of the Sleeper deposit, Humboldt, County, Nevada: epithermal gold–silver mineralization following silicic flow-dome complex. *Economic Geology*, v. 88, p. 317–327.
- Cox, D.P., and Singer, D.A., 1990. Descriptive and grade-tonnage models for distal-disseminated Ag-Au deposits. *A supplement to U.S. Geological Survey Bulletin 1693*: U.S. Geological Survey Open-File Report 90-282, p. 7.
- Cox, D.P., 1992. Descriptive model of distal disseminated Ag-Au, in Bliss, J.D., ed., *Developments in deposit modeling U.S. Geological Survey Bulletin 2004*, p. 19.
- Craig, H., Boato, G., and White, D.E., 1956. Isotopic geochemistry of thermal waters. *Proceedings of Conference of Nuclear Processes in Geologic Environments, Second National Academy of Sciences-National Resource Council*, pub. 400.
- Cline, J.S., Hofstra, A.H., Muntean, J.L., Tosdal, R.M., and Hickey, K.A., 2005. Carlin-Type Gold Deposits in Nevada: Critical Geologic Characteristics and Viable Models. *Economic Geology*, 100th Anniversary Volume, p. 451-484.
- Day, J.M.D., 2013. Hotspot volcanism and highly siderophile elements. *Chemical Geology*, v. 341, p. 50-74.
- Day, J.M.D., Pearson D.G., Hulbert L. J., 2013. Highly siderophile element behavior during flood basalt genesis and evidence for melts from intrusive chromitite formation in the Mackenzie large igneous province. *Lithos*. p. 182-183:242-258.
- Day, J.M.D., Waters C.L., Schaefer B.F., Walker R.J., Turner S., 2016. Use of Hydrofluoric Acid Desilicification in the Determination of Highly Siderophile Element Abundances and Re-Pt-Os Isotope Systematics in Mafic-Ultramafic Rocks. *Geostandards and Geoanalytical Research*.
- Day, J.M.D., Brandon, A.D., R.J. Walker., 2016. Highly siderophile elements in Earth, Mars, the Moon, and asteroids. *Rev. Mineral. Geochem.*, v. 81, pp. 161-238.
- Day, J.M.D., Maria-Benavides J., McCubbin F.M., Zeigler R.A., 2018. The potential for metal contamination during Apollo lunar sample curation. *Meteoritics and Planetary Science*.
- Dickinson, W.R., and Snyder, W.S., 1979. Geometry of Subducted Slabs Related to San Andreas transform, *The Journal of Geology*, v. 87, p. 609-627.
- Elwell, C.K., 2011. A Brief History of the Gold Standard in the United States. *Congressional Research Service Report for Congress*. No. R41887.

- Feeley, T.C., and Grunder, A L., 1991. Mantle contribution to the evolution of middle Tertiary silicic magmas during early stages of extension: The Egan Range Volcanic Complex, east-central Nevada. *Contributions of Mineralogy and Petrology*, p. 106:154-169.
- Friedman, M., and Jacobson Schwartz, A., 1963. A Monetary History of the United States, 1867-1960. *Princeton University Press*.
- Eichengreen, B., and Temin., P., 2000. The Gold Standard and the Great Depression. *Contemporary European History*, vol. 9, no. 2, p. 183–207.
- Gammons, C. H., Williams-Jones, A. E., 1995. Hydrothermal geochemistry of electrum; thermodynamic constraints. *Economic Geology* ; v.90, n. 2, p.420–432.
- Geist, D., and Richards, M., 1993. Origin of the Columbia River plateau and Snake River plain: Deflection of the Yellowstone plume. *Geology*, v. 21, p. 789–792.
- Glen, J.M.G., and Ponce, D.A., 2002. Large-scale fractures related to inception of the Yellowstone hotspot. *Geology*, v. 30.7, p. 647-6.
- Godel, B., Barnes, S.J., 2008. Platinum-group elements in sulfide minerals and the whole rocks of the J-M Reef (Stillwater Complex): Implication for the formation of the reef, *Chemical Geology*, v. 248, Issues 3–4, Pages 272-294.
- Günther, D., Audétat, A., Frischknecht, R., and Heinrich, C.A., 1998. Quantitative analysis of major, minor and trace elements in fluid inclusions using laser ablation-inductively coupled plasma-mass spectrometry (LA-ICP-MS). *Journal of Analytical Atomic Spectroscopy*, v. 13, p. 263–270.
- Halsor SP, Bornhorst TJ, Beebe M, Richardson K, Strowd W (1988) Geology of the DeLamar silver mine, Idaho—a volcanic dome complex and associated hydrothermal system. *Economic Geology*, v. 83, p.1159–1169.
- Harvey, J, Day, J.M.D., 2016. Highly siderophile and strongly chalcophile elements in high temperature geochemistry and cosmochemistry. *Mineralogical Society of America*, v. 81, p. 774.
- Hames, W., Unger, D., Saunders, J., Kamenov, G., 2009. Early Yellowstone hotspot magmatism and gold metallogeny: *Journal of Volcanology and Geothermal Research*, v. 188, p. 214 – 224.
- Hedenquist, J.W., and Lowenstern, J.B., 1994. The role of magmas in forming hydrothermal ore deposits. *Nature*, v. 370, p. 519–527.
- Hofstra, A.H., Wallace, A.R., 2006. Metallogeny of the great basin: crustal evolution, fluid flow, and ore deposits. *US Geological Survey*.
- Hooper, P.R., 2000, Chemical discrimination of Columbia River basalt flows: *Geochemistry, Geophysics, Geosystems*, v. 1 (6), doi: 10.1029/2000GC000040.

- Hooper, P.R., Binger, G.B., and Lees, K.R., 2002a, Ages of the Steens and Columbia River flood basalts and their relationship to extension-related calc-alkalic volcanism in eastern Oregon: *Geological Society of America Bulletin*, v. 114, p. 43-50. (Corrections p. 923-924).
- Hudson, D.M., John, D.A., Fleck, R.J., 2006. Geology, geochemistry, and geochronology of epithermal deposits in the Seven Troughs district, Pershing County, Nevada. *Geol. Soc. Nev. Special Publication*, v. 42, p. 110–126.
- John, D.A., Hofstra, A.H., Fleck, R.J., Brummer, J.E., Saderholm, E.C., 2003a. Geologic setting and genesis of the Mule Canyon low-sulfidation epithermal gold- silver deposit, north-central Nevada, *Economic Geology*, v. 98, p. 425–464.
- John, D.A., Hofstra, A.H., Theodore, T.G., 2003b. A Special Issue Devoted to Gold Deposits in Northern Nevada: Part 1. Regional Studies and Epithermal Deposits, *Economic Geology*, v. 98, no. 2, p. 225-234.
- John, D.A., and Wallace, A.R., 2000. Epithermal gold-silver mineral deposits related to the northern Nevada rift: Geological Society of Nevada, *Geology and Ore Deposits 2000: the Great Basin and Beyond Symposium*, Reno-Sparks, Nevada, Proceedings, p. 155–175.
- Large, D.E., 1981. Sediment-hosted Submarine Exhalative Lead–zinc Deposits – A Review Of Their Geological Characteristics And Genesis. Regional and Specific Deposits, p. 469-907.
- Leavitt, E.D., Spell, T.L., Goldstrand, P.M., and Arehart, G.B., 2004. Geochronology of the Midas Low-Sulfidation Epithermal Gold-Silver Deposit, Elko County, Nevada, *Economic Geology*, v. 99, p. 1665-1686.
- Liu, L., and Stegman, D.R., 2012, Origin of Columbia River flood basalt controlled by propagating rupture of the Farallon slab. *Nature*, v. 482, p. 386–389.
- Meisel, T., Walker, R.J., Irving, A.J., Lorand, J.-P., 2001. Osmium isotopic compositions of mantle xenoliths: a global perspective. *Geochimica et Cosmochimica Acta*, v. 65, p.1311-1323.
- Millard, J.B., Muntean, J.L., Marma, J.C., 2018. Genetic Links between the Development of Extensional Basins and the Formation of Low Sulfidation Epithermal Deposits. *CREG Report*.
- Muntean, J.S., Cline, J.S., Simon, A.C., Longo, A.A., 2011. Magmatic–Hydrothermal Origin of Nevada’s Carlin-Type Gold Deposits.” *Nature Geoscience*, vol. 4, no. 2, p. 122–127.
- Morris, G.A., Larson, P.B., and Hooper, P.R., 2001. “Subduction style” magmatism in a non-subduction setting: the Colville Igneous Complex, NE Washington state, USA. *Journal of Petrology*, v. 41, p. 43–67.
- Nash, J.T., Utterback, W.C., and Trudel, W.S., 1995. Geology and geochemistry of Tertiary volcanic host rocks, Sleeper Gold-Silver deposit, Humboldt County, Nevada. *U.S. Geological Survey Bulletin*, 2090.

- Nekrasov, I. YA., 1996. *Geochemistry, Mineralogy and Genesis of Gold Deposits*. Xiv 329 Pp. Rotterdam, Brookfield: A. A. Balkema. Print.
- Noble, D.C., McCormack, J.K., McKee, E.H., Silberman, M.L., and Wallace, A.B., 1988. Time of mineralization in the evolution of the McDermitt caldera complex, Nevada-Oregon, and the relation of middle Miocene mineralization in the northern Great Basin to coeval regional basaltic magmatic activity, *Economic Geology*, v. 83, p. 859–863.
- Odell, M. A., Swanson, K., White, M., 2013. NI 43-101 Technical Report, Fire Creek Exploration Project, Lander County, Nevada. NI 43- 101, Technical Report.
- Odell, M. A., Symmes, L., Bull, S., and Swanson, K., July 24, 2014. Preliminary Economic Assessment of the Fire Creek Project, Lander County, Nevada, Amended. NI 43-101, Technical Report.
- Odell, M., Symmes, L., Bull, S., Knight, A., 2018. Technical Report for the Fire Creek Project, Lander County, Nevada.
- Peters, BJ, Day, J.M.D., 2014. Assessment of relative Ti, Ta, and Nb (TITAN) enrichments in ocean island basalts. *Geochemistry, Geophysics, Geosystems*.
- Pettke, T. and Frei, R. 1996. Isotope systematics in vein gold from Brusson, Val d’Ayas (NW Italy), 1. Pb/Pb evidence for a Piemonte metaophiolite Au source. *Chemical Geology*. v. 127, p.111-124.
- Pirajno, F., 2009. *Hydrothermal processes and mineral systems*. Print.
- Ponce, D.A., and Glen, J.M.G., 2008. A prominent geophysical feature along the northern Nevada rift and its geologic implications, north-central Nevada. *Geosphere*, v. 4.1, p. 207-217.
- Reidel, S.P., Camp, V.E., Ross, M.E., Wolf, J.A., Martin, B.S., Tolan, T.L., Wells, R.E., 2013. The Columbia River Flood Basalt Province. *Geological Society of America*.
- Robinson, E.S., 1970. Relations between geological structure and aeromagnetic anomalies in central Nevada. *Geological Society of America Bulletin*, 81.7.
- Rudnick, R.L. and Gao, S., 2003. Composition of the Continental Crust. *Treatise on Geochemistry*, v. 3, p.659.
- Rye, R.O , 1966. The carbon, hydrogen, oxygen isotopic composition of the hydrothermal solutions responsible for the lead-zinc deposits at Providencia, Zacatecas, Mexico. *Economic Geology*, v. 61, p. 1399–1427.
- Saal, A. E., Rudnick, R. L., Ravizza, G. E., and Hart, S. R., 1998. Re-Os isotope evidence for the composition, formation and age of the lower continental crust, *Nature*, v. 393, p. 58 – 61.

- Saunders, J.A., and Crowe, D.E., 1996, Retardation of boiling and the genesis of shallow Bonanza epithermal gold deposits: Evidence from the Sleeper deposit, Nevada [abs.]: *Geological Society of America Abstracts with Programs*, v. 28, no.7, p. 94.
- Saunders, J.A., and Schoenly, P.A., 1995, Boiling, colloid nucleation and aggregation, and the genesis of bonanza gold mineralization at the Sleeper Deposit, Nevada. *Mineralium Deposita*, v. 30, p. 199–211.
- Sillitoe, R.H., and Bonham, H.F., 1990, Sediment-hosted gold deposits: Distal products of magmatic-hydrothermal systems: *Geology*, v. 18, p. 157–161.
- Sillitoe, R. H., Hannington, M. D., & Thompson, J. F., 1996, High sulfidation deposits in the volcanogenic massive sulfide environment. *Economic Geology*, v. 91, p. 204-212.
- Sun, W., Huang, R., Li, H., Hu, Y., Zhang, C., Sun, S., Zhang, L., Ding, X., Li, C., Zartman, R. and Ling, M. (2015). Porphyry deposits and oxidized magmas. *Ore Geology Reviews*, v. 65, p. 97-131.
- Swisher, C.C., Ach, J.A., and Hart, W.K., 1990, Laser fusion $^{40}\text{Ar}/^{39}\text{Ar}$ dating of the type Steens Mountain Basalt, southeastern Oregon and the age of the Steens geomagnetic polarity transition: *Eos (Transactions, American Geophysical Union)*, v. 71, Fall Meeting Supplement, p. 1296.
- Taylor, H.P., 1973, O18/O16 evidence for meteoric-hydrothermal alteration and ore deposition in the Tonopah, Comstock Lode, and Goldfield mining districts, Nevada. *Economic Geology*, v. 68, p. 747–764.
- Tolan, T.L., Reidel, S.P., Beeson, M.H., Anderson, J.L., Fecht, K.R., and Swanson, D.A., 1989, Revisions to the estimates of the areal extent and volume of the Columbia River Basalt Group, in Reidel, S.P., and Hooper, P.R., eds., *Volcanism and tectonism in the Columbia River flood-basalt province: Geological Society of America Special Paper 239*, p. 1-20.
- Tosdal, R.M., Cline, J.S., Fanning, C.M., and Wooden, J.L., 2003. Lead in the Getchell-Turquoise Ridge Carlin-type gold deposits from the perspective of potential igneous and sedimentary rock sources in northern Nevada: Implications for fluid and metal sources. *Economic Geology*, v. 98, p. 1189–1211.
- Theodore, T.G., Armstrong, A.K., Harris, A.G., Stevens, C.G., and Tosdal, R.M., 1998. Geology of the northern terminus of the Carlin trend, Nevada—links between crustal shortening during the Late Paleozoic Humboldt orogeny and northeast-striking faults, *U.S. Geological Survey Open- File Report 98-338*, p. 69– 105.
- Theodore, T.G., 1998. Large Distal-Disseminated Precious Metal Deposits, Battle Mountain Mining District, Nevada. *U.S. Geological Survey Open-File Report 98-338*, p. 253-258.
- Theodore, T.G., 2000. Geology of pluton-related gold mineralization at Battle Mountain, Nevada. *Monographs in Mineral Resource Science*, No. 2, Center for Mineral Resources, p. 271.

- Vikre, P.G., 1985. Precious metal vein system in the National district, Humboldt County, Nevada. *Economic Geology*, v. 80, p. 360–393.
- Wallace, A.R., 2003. Geology of the Ivanhoe Hg-Au district, northern Nevada: Influence of Miocene volcanism, lakes, and active faulting on epithermal mineralization, *Economic Geology*, 98, p. 409–424.
- Wells, J.D., Elliott, J.E., and Obradovich, J.D., 1971, Age of the igneous rocks associated with ore deposits, Cortez-Buck horn area, Nevada. *U.S. Geological Survey Professional Paper* 750-C, p. C127-C135.
- Weaver, B.L. and Tarney, J. (1984). Major and trace element composition of the continental lithosphere. *Physics and Chemistry of the Earth*, v.15, p. 39-68.
- Zoback, M.L., McKee, E.H., Blakely, R.J., and Thompson, G.A., 1994. The northern Nevada rift: Regional tectono-magmatic relations and middle Miocene stress direction, *Geological Society of America Bulletin*, v. 106, 371–382.
- Zoback, M. L., & Thompson, G. A., 1978. Basin and Range rifting in northern Nevada: Clues from a mid-Miocene rift and its subsequent offsets, *Geology*, v. 6, p. 111- 116.

Tables

Table 2: Laser-ablation ICP-MS data (ppm) for standard reference materials, Hoba, Filomena and Coahuila

Sample ID	Au	Re	Pd	Pt	Rh	Ru	Ir	Os
HOBA								
FC50-1-2	0.066 <i>0.01</i>	2.81 <i>0.30</i>	10.70 <i>1.39</i>	29.40 <i>5.19</i>	3.54 <i>0.38</i>	29.30 <i>2.89</i>	27.90 <i>3.41</i>	38.40 <i>4.23</i>
FC50-1-3-1	0.064 <i>0.011</i>	2.81 <i>0.32</i>	10.70 <i>1.75</i>	29.40 <i>2.91</i>	3.54 <i>0.60</i>	29.30 <i>4.38</i>	27.90 <i>2.87</i>	38.40 <i>4.50</i>
FC50-1-3-2	0.049 <i>0.070</i>	2.81 <i>0.03</i>	10.70 <i>1.13</i>	22.70 <i>4.68</i>	3.54 <i>0.47</i>	36.23 <i>8.52</i>	27.90 <i>1.03</i>	38.40 <i>1.40</i>
FC50-2-1	0.056 <i>0.008</i>	2.03 <i>0.05</i>	9.45 <i>0.70</i>	26.18 <i>1.30</i>	3.48 <i>0.07</i>	24.38 <i>1.04</i>	22.72 <i>0.82</i>	26.93 <i>0.67</i>
Recommended Hoba	0.064	2.81	10.7	29.4	3.54	29.3	27.9	38.4
FILOMENA								
FC50-1-2	0.26 <i>0.17</i>	0.08 <i>0.04</i>	1.72 <i>0.63</i>	14.13 <i>5.64</i>	1.22 <i>0.48</i>	9.41 <i>3.66</i>	1.81 <i>0.73</i>	0.53 <i>0.28</i>
FC50-1-3-1	0.14 <i>0.06</i>	0.09 <i>0.02</i>	1.40 <i>0.68</i>	11.95 <i>6.05</i>	1.20 <i>0.54</i>	8.83 <i>4.12</i>	1.71 <i>0.88</i>	0.54 <i>0.30</i>
FC50-1-3-2	0.45 <i>0.15</i>	0.19 <i>0.03</i>	3.24 <i>0.73</i>	14.06 <i>2.47</i>	2.07 <i>0.38</i>	23.20 <i>3.89</i>	3.04 <i>0.52</i>	0.88 <i>0.14</i>
FC50-2-1	0.61 <i>0.12</i>	0.13 <i>0.01</i>	2.89 <i>0.22</i>	19.78 <i>1.85</i>	2.16 <i>0.13</i>	14.01 <i>1.32</i>	2.68 <i>0.17</i>	0.64 <i>0.03</i>
Recommended Filomena	0.61	0.25	2.7	24.3	2.86	17.8	5.2	1.0
COAHUILA								
FC50-1-2	1.24 <i>0.84</i>	1.27 <i>0.05</i>	3.52 <i>0.54</i>	42.23 <i>3.55</i>	2.78 <i>0.21</i>	26.11 <i>0.28</i>	19.48 <i>1.70</i>	10.91 <i>0.78</i>
FC50-1-3-1	0.85 <i>0.20</i>	1.13 <i>0.30</i>	3.40 <i>0.93</i>	29.55 <i>9.32</i>	2.65 <i>0.19</i>	25.83 <i>3.47</i>	15.47 <i>4.71</i>	8.73 <i>2.72</i>
FC50-1-3-2	0.61 <i>0.10</i>	1.56 <i>0.17</i>	3.26 <i>0.66</i>	24.30 <i>3.27</i>	3.02 <i>0.47</i>	40.66 <i>5.66</i>	20.62 <i>2.33</i>	12.98 <i>1.34</i>
FC50-2-1	0.85 <i>0.20</i>	1.13 <i>0.30</i>	3.40 <i>0.93</i>	29.55 <i>9.32</i>	2.65 <i>0.19</i>	25.83 <i>3.47</i>	15.47 <i>4.71</i>	8.73 <i>2.72</i>
Recommended Coahuila	0.49	1.08	2.5	31.2	2.98	23.2	16.3	8.5

Table 3 (continued)

Sample ID	BHVO-2		BIR-1		BCR-2		TPB
	(n = 8)	2StDev	(n = 8)	2StDev	(n = 6)	2StDev	(n = 8)
Li	4.90	0.28	3.17	0.46	9.33	0.97	0.0089
Sc	32.40	1.07	39.41	7.71	31.95	2.64	0.0083
Ti	16575	936	5943	459	12552	1333	0.0223
V	322.95	21.37	328.01	25.75	389.54	46.04	0.0182
Cr	285.31	19.85	377.10	43.12	13.76	1.70	0.0723
Mn	1338	78	1325	132	1465	150	0.0503
Co	45.93	3.48	53.49	4.39	35.36	4.63	0.0612
Ni	121.41	8.88	178.89	13.40	11.64	1.47	0.0164
Cu	129.38	9.72	119.44	9.05	18.84	2.11	0.0673
Zn	104.15	6.34	68.99	5.69	118.07	19.96	3.2812
Rb	9.14	0.27	0.15	0.06	45.57	3.03	0.0060
Sr	396.47	7.49	97.08	13.88	329.42	19.43	0.0175
Y	26.06	0.45	13.76	2.12	34.61	2.16	0.0022
Zr	172.72	3.74	13.61	1.08	181.03	11.88	0.0671
Nb	18.29	0.31	0.52	0.05	11.70	0.89	0.0010
Ba	130.11	1.59	6.23	0.55	673.17	31.64	0.4836
La	15.17	0.38	0.56	0.09	24.30	1.36	0.0018
Ce	37.41	1.06	1.77	0.20	51.34	2.92	0.0052
Pr	5.34	0.10	0.35	0.05	6.68	0.36	0.0007
Nd	24.42	0.59	2.21	0.30	28.07	1.47	0.0027
Sm	6.05	0.15	1.01	0.13	6.42	0.33	0.0005
Eu	2.06	0.07	0.49	0.05	2.05	0.12	0.0001
Gd	6.22	0.29	1.55	0.20	6.73	0.40	0.0005
Tb	0.92	0.04	0.32	0.04	1.01	0.06	0.0001
Dy	5.29	0.23	2.36	0.30	6.25	0.34	0.0004
Ho	0.98	0.04	0.52	0.07	1.26	0.07	0.0001
Er	2.53	0.10	1.54	0.20	3.57	0.20	0.0001
Tm	0.33	0.02	0.23	0.03	0.51	0.03	0.0000
Yb	1.99	0.10	1.50	0.21	3.27	0.19	0.0001
Lu	0.27	0.01	0.22	0.03	0.48	0.03	0.0000
Hf	4.33	0.23	0.56	0.04	4.72	0.28	0.0010
Ta	1.13	0.06	0.04	0.00	0.74	0.05	0.0002
W	0.21	0.02	0.03	0.01	0.42	0.03	0.0085
Pb	1.59	0.10	2.92	0.33	11.18	1.06	0.1087
Th	1.22	0.09	0.03	0.01	5.66	0.45	0.0002
U	0.40	0.03	0.01	0.00	1.55	0.12	0.0001

Table 4: Osmium isotope and HSE abundances (pg) for total analytical blanks

Sample ID	Type	Re	Pd	Pt	Ru	Ir	Os	$^{187}\text{Os}/^{188}\text{Os}$	2SE
JMB3-1	Blank - Country Rocks	7.00	13.00	0.40	10.00	2.50	0.80	0.1713	0.007
JMB2-2	Blank - Standard	1.10	21.00	2.00	14.00	2.50	0.60	0.1700	0.006
JMB4-1	Blank - Electrum	0.50	6.30	2.00	19.00	1.00	1.30	0.1384	0.002
	<i>Ave.</i>	2.87	13.43	1.47	14.3	2.0	0.9	0.1599	0.005
	<i>ISE</i>	3.59	7.36	0.92	4.51	0.87	0.36	0.02	
	<i>RSD%</i>	1.25	0.55	0.63	0.31	0.43	0.40	0.12	

Table 5: Analysis of in-house metal and sulfide standards versus recommended values

	Hoba IVB Metal H		Filomena IIAB Metal C		Coahuila IIAB Metal F		Stillwater Sulfide
ppm							
Cr	195.5		75.72		89.70		11.53
Co	5706		3538		3486		1604
Ni	146007	166000	51731	56500	51698	55000	112471
Cu	7.0		122.7		131.4		179.6
Zn	1.1		4.4		1.4		28.6
Ga	0.28		60.9		62.7		0.14
Ge	5.98		66.6		67.8		3.68
Se	3.19		3.03		2.57		
Nb	1.37		0.81		0.44		0.19
Mo	34.3		11.5		8.91		1.82
Sn	0.21		1.09		1.45		1.08
Te	0.001		0.004		0.003		0.784
W	3.48		2.77		3.18		0.11
Tl	0.07		0.02		0.05		2.28
Pb	0.07		0.05		0.11		6.32
ppb							
Au	123		855		823		73.2
Re	2810	2731	249	200.0	1081	1228	323
Pd	10677	6244	2726		2531		814000
Pt	29361	30780	24288	25340.0	62447	32170	1174
Ru	29279	29150	17794		23226		5589
Ir	27917	27570	5225		16326		4086
Os	38448	39218	1003	1030.0	8545	10138	2753
$^{187}\text{Re}/^{188}\text{Os}$	0.1031		0.3259		0.1615		0.0628
2SE	0.0015		0.0049		0.0024		0.0009
$^{187}\text{Os}/^{188}\text{Os}$	0.121904	0.12188	0.16927	0.16932	0.15248	0.14163	0.15012
2SE	0.000008		0.00021		0.00072		0.00013

Table 6: Laser-ablation ICP-MS data (in ppm) for sulfide samples from JM Reef at the Stillwater Mine, MT

Sample ID	Au	Re	Pd	Pt	Rh	Ru	Ir	Os
JM-Reef Sulfide								
JMR_1	2931	0.17	43116	26.43	647	102	65.56	7.72
JMR_2_1	1677	0.10	8152	8.03	1.94	1.36	1.21	0.09
JMR_2_2	2394	0.07	25412	15.07	31.82	2.60	6.15	0.07
JMR_3	419	2.11	46.63	1.33	0.72	1.12	4.47	0.50
JMR_4	1273	4.68	204	2.24	2.31	3.54	8.94	1.43
JMR_5	3079	0.79	103	0.32	1.26	1.98	7.53	0.39
JMR_6_1	4564	0.34	736	9.22	10.68	12.60	11.67	2.32
JMR_6_2	3069	0.04	75.30	0.45	0.87	1.47	7.20	0.40
JMR_7	419	0.03	24.87	0.58	0.59	1.85	6.80	0.30
JMR_8	6739	2.24	74.93	0.99	1.37	3.06	11.70	0.97
JMR_9	12889	2.75	117	1.12	1.70	2.97	9.97	0.93
JMR_10_1	5504	3.55	49137	26.78	178	6.53	23.89	1.51
JMR_10_2	5638	1.29	26157	19.19	5.37	4.32	2.94	0.33
JMR_11	3007	2.76	41015	23.38	304	20.25	28.41	2.61
JMR_12_1	2794	0.07	21611	13.10	10.46	1.71	1.17	0.14
JMR_12_2	1300	0.08	37928	21.88	152	3.91	17.50	0.61
JMR_13_1	16	0.09	12104	7.61	221	61.22	22.70	7.23
JMR_13_2	836	0.05	33539	17.42	535	154	51.22	14.82
JMR_14	3583	0.00	28.40	0.22	0.55	0.73	2.53	0.08
JMR_16_1	1578	0.02	154	2.47	1.60	0.88	2.73	0.21
JMR_16_2	9220	8.31	37705	31.57	148	9.54	20.39	2.79
JMR_17	889	0.45	51669	26.78	654	60.71	68.12	7.69
JMR_18_1	1732	0.02	161	2.55	1.37	2.25	4.52	0.60
JMR_18_2	1490	0.00	87.85	6.85	1.17	3.65	4.07	0.29
JMR_19	3422	0.05	105	0.83	2.00	3.58	10.03	0.54
JMR_20_1	2911	0.79	34.49	0.50	0.68	1.22	4.02	0.33
JMR_20_2	2326	5.57	19639	10.44	146	6.31	19.81	1.96
Hoba	0.01	2.81	10.70	29.40	3.54	29.30	27.90	38.40
<i>St. Dev.</i>	<i>0.02</i>	<i>0.23</i>	<i>0.51</i>	<i>1.20</i>	<i>0.12</i>	<i>1.88</i>	<i>1.90</i>	<i>2.92</i>
Filomena	0.80	0.22	3.77	26.59	2.58	19.91	3.94	1.11
<i>St. Dev.</i>	<i>0.13</i>	<i>0.03</i>	<i>0.13</i>	<i>0.67</i>	<i>0.03</i>	<i>0.97</i>	<i>0.31</i>	<i>0.08</i>
Coahuila	4.92	1.47	3.17	34.75	2.84	26.66	19.25	10.97
<i>St. Dev.</i>	<i>2.93</i>	<i>0.19</i>	<i>0.12</i>	<i>4.25</i>	<i>0.28</i>	<i>1.52</i>	<i>1.86</i>	<i>1.08</i>

Table 7: Full 187Re-187Os isotope and highly siderophile element abundances (ppb) for Fire Creek electrum and country rocks

Sample ID	Type	Re	Re blk %	Pd	Pd blk %	Pt	Pt blk %	Ru	Ru blk %	Ir	Ir blk %	Os	Os blk %	¹⁸⁷ Re/ ¹⁸⁷ Os	2SE	¹⁸⁷ Os/ ¹⁸⁸ Os	2SE
FC50-2-1 Au III	Electrum	1.69	1.6%	2.5	1.0%	22.3	3.6%	1.2	16%	0.55	2.7%	0.0421	0.3%	387	6	0.1454	0.0022
FC50-2-1 Au III	Electrum	0.31	3.4%	1.8	0.5%	14.9	2.0%	1.8	40%	0.37	1.5%	0.2063	4%	78	1	0.2107	0.0043
FC50-1-3-2	Electrum	1.64	0.3%	23.2	8.5%	12.47	5.5%	20.24	30%	0.22	90%	0.0223	13%	1180	18	0.5584	0.0065
FC50-1-2	Electrum	2.59	0.6%	12.5	5.6%	14.31	1.7%	7.12	31%	0.99	11%	0.0158	9%	3364	50	0.8800	0.0091
FC50-2-1a	Electrum	5.03	0.1%	3.2	10.0%	53.50	0.2%	1.13	87%	0.54	9%	0.0180	7%	2284	34	0.7310	0.0063
FC50-2-1b	Electrum	3.96	0.2%	2.8	11.0%	74.88	0.1%	1.36	69%	0.28	17%	0.0091	14%	2568	39	0.6431	0.0051
FC50-1-3-2a	Electrum	2.26	0.3%	2.9	10.7%	56.00	0.2%	1.56	61%	3.64	1%	0.0211	6%	1178	18	0.3406	0.0029
FC50-1-3-2b	Electrum	2.51	0.2%	2.6	11.0%	95.66	0.1%	0.85	86%	6.84	1%	0.0202	2%	199	3	1.2186	0.0030
FC47-1-2	Dike	0.731	0.3%	12.81	0%	0.125	2.2%	0.263	9%	0.0960	5%	0.0029	16%	1304	20	0.9141	0.0068
702-3	Tbeq	0.701	0.1%	3.82	1%	0.043	3.5%	0.101	12%	0.0147	16%	0.0235	2%	25	0	0.5198	0.0015
427-1	LAT	0.117	0.9%	0.004	75%	0.019	7.7%	0.107	12%	0.0025	50%	0.0033	15%	4788	72	1.7819	0.0019
427-2	Tbma	2.668	0.4%	0.011	50%	0.394	0.4%	0.096	13%	0.0046	50%	0.0052	10%	92	1	0.3384	0.0063
427-6	T&B	0.097	1.1%	0.006	75%	0.112	1.3%	0.120	10%	0.0016	50%	0.0211	3%	120	2	0.8163	0.0238
427-7	Dike	0.482	0.2%	1.28	2%	0.024	6.6%	0.151	9%	0.0464	5%	0.0024	18%	1041	16	0.8659	0.0042
427-9	Dike	0.477	0.2%	1.40	1%	0.349	0.4%	0.138	9%	0.0020	50%	0.0260	2%	122	2	0.5875	0.0026
427-10	T&B	0.619	0.2%	1.44	1%	0.056	2.9%	0.147	9%	0.0028	89%	0.0024	2%	122	2	0.5875	0.0026

Table 8: Laser-ablation ICP-MS data (in ppm) for gold samples from the Fire Creek Mine, NV

Sample ID	Au	Re	Pd	Pt	Rh	Ru	Ir	Os
Sample 50-1-2-2								
FC50-1-2-2_1	757163	0.019		0.124			0.023	0.022
FC50-1-2-2_2	685349	0.009	6.872	0.096	0.044		0.000	0.019
FC50-1-2-2_3	719616	0.018	0.134	0.175	0.018	0.106	0.007	
FC50-1-2-2_4	667343	0.002	0.143	0.059	0.176		0.307	
FC50-1-2-2_5	684552		0.150	0.280	0.021	0.059	0.047	
FC50-1-2-2_6	634481			0.368		0.111	0.007	
FC50-1-2-2_7	612802		0.070				0.362	
FC50-1-2-2_8	665774	0.011	0.082	0.014	0.034		0.034	
FC50-1-2-2_9	673485		0.158					
FC50-1-2-2_10	599074		0.145	0.027	0.001		0.617	
FC50-1-2-2_11	596165	0.019			0.010	0.057	0.007	0.043
FC50-1-2-2_12	825908	0.002	0.078	0.058	0.011	0.062	0.016	0.023
FC50-1-2-2_13	866644		0.403	0.025	0.009	0.053	0.021	0.040
FC50-1-2-2_14	826860	0.010	0.076	0.020		0.121		
FC50-1-2-2_15	684783	0.027	0.067	0.226	0.018		0.021	
Sample 50-1-3-1								
FC50-1-3-1_1	755020		0.051	0.078	0.003	0.016	0.113	0.018
FC50-1-3-1_2	732895	0.002	0.049		0.010			
FC50-1-3-1_3	748204		0.117	0.157		0.014		0.006
FC50-1-3-1_4	720472		0.033	0.023			0.002	0.005
FC50-1-3-1_5	721968		0.032	0.023				
FC50-1-3-1_6	733895	0.002	0.016	0.030		0.055	0.020	
FC50-1-3-1_7	645337	0.002	0.035	0.008	0.015		0.002	0.005
FC50-1-3-1_8	692800	0.017	0.038		0.006			
FC50-1-3-1_9	740701		0.066	0.071			0.009	0.005
FC50-1-3-1_10	731966	0.017	0.073	0.026	0.004	0.020	0.005	0.008
FC50-1-3-1_11	654721	0.005	0.058	0.035	0.009	0.016	0.004	0.012
FC50-1-3-1_12	582993	0.021	0.095		0.006		0.023	0.024
FC50-1-3-1_13	639029		0.056	0.034			0.002	
Sample 50-1-3-2								
FC50-1-3-2_1	779772		0.242	0.098		0.163		0.104
FC50-1-3-2_2	692741	0.066	0.344	0.076	0.022		0.070	0.059
FC50-1-3-2_3	725086		0.439	0.024			0.071	0.279
FC50-1-3-2_4	708130	0.020	0.101					
FC50-1-3-2_5	701006				0.012	0.248	0.036	0.081
FC50-1-3-2_6	685811	0.066		0.032		0.141	0.012	0.079
FC50-1-3-2_7	641097		0.356					
FC50-1-3-2_8	692969	0.039	0.511	0.000	0.057	0.403	0.031	0.039
FC50-1-3-2_9	712963	0.040	0.543	0.019		0.174		0.042
FC50-1-3-2_10	660424	0.067				0.153	0.024	

Table 8: (continued)

Sample ID	Au	Re	Pd	Pt	Rh	Ru	Ir	Os
Sample 50-2-1								
FC50-2-1_1	726511	0.825	0.866		0.014		0.087	
FC50-2-1_2	875192	2.537	1.167	1.341	0.086	0.186	0.093	0.011
FC50-2-1_3	700706	0.704	0.802	0.529	0.068		0.047	
FC50-2-1_4	789689	0.542	1.899	1.933	0.060	0.128	0.061	0.020
FC50-2-1_5	765148	0.652	0.990	1.422	0.128	0.155	0.537	
FC50-2-1_6	821259	0.732	1.300	1.329	0.052	0.102	0.229	0.037
FC50-2-1_7	582900	0.337	0.835	0.512	0.037		0.040	0.077
FC50-2-1_8	496131	0.132	0.907	0.177	0.020	0.059	0.106	0.045
FC50-2-1_9	741255	1.132	0.738	0.621	0.069	0.083	0.143	
FC50-2-1_10	592566	0.391	0.605	0.535	0.022	0.165	0.367	0.012
FC50-2-1_11	608643	0.952	0.223	0.161	0.017	0.129	1.993	
Sample 50-1 from Perez (2013)								
	EMPA							
Fe15a05	733216	0.192	0.653	4.932	0.022	0.138	0.367	0.367
Fe15a06	698379	0.188	0.715	4.932	0.026	0.136	0.410	0.399
Fe15a07	656363	0.169	0.538	4.944	<0.03	<0.14	0.378	0.462
Fe15a08	697876	0.153	0.738	4.681	<0.07	<0.17	0.327	0.359
Fe15a09	627540	0.209	0.581	4.828	0.037	0	0.438	0.386
Fe15a10	680229	0.151	0.753	4.564	<0.04	<0.30	0.325	0.275
Fe15a11	713250	0.177	0.744	5.073	<0.03	<0.18	0.384	0.408
Fe15a12	723910	0.133	0.895	4.741	0.042	0.087	0.414	0.409
Fe15d05	676937	0.150	0.735	5.002	<0.03	0.094	0.268	<0.27
Fe15d06	571340	0.155	0.669	4.686	<0.11	0.079	0.328	0.354
Fe15d07	668516	0.099	0.624	4.429	0.035	0.098	0.302	0.331
Fe15d08	689962	0.099	0.516	5.120	0.028	0.083	0.315	0.360
Fe15d09	688813	0.166	0.759	4.853	0.021	0.135	0.284	0.378
Fe15d10	675101	0.166	0.707	4.983	<0.04	<0.19	0.327	0.406
Fe15d11	675101	0.158	0.624	4.872	0.039	0.064	0.306	0.375
Fe15d12	725132	0.106	0.711	5.091	<0.04	<0.42	0.331	0.386
Fe15d13	754786	0.145	0.834	4.827	<0.05	<0.19	0.380	0.365
Fe15d14	735628	0.175	0.744	5.140	<0.09	<0.21	0.363	0.413
Fe15d15	723002	0.123	<0.85	5.039	0.032	<0.17	0.348	0.274
Fe15d16	728186	0.110	0.416	4.221	0.034	<0.24	0.250	0.358